

# Rheology of Unentangled Polymer Solutions Depends on Three Macromolecular Properties: Flexibility, Extensibility, and Segmental Dissymmetry

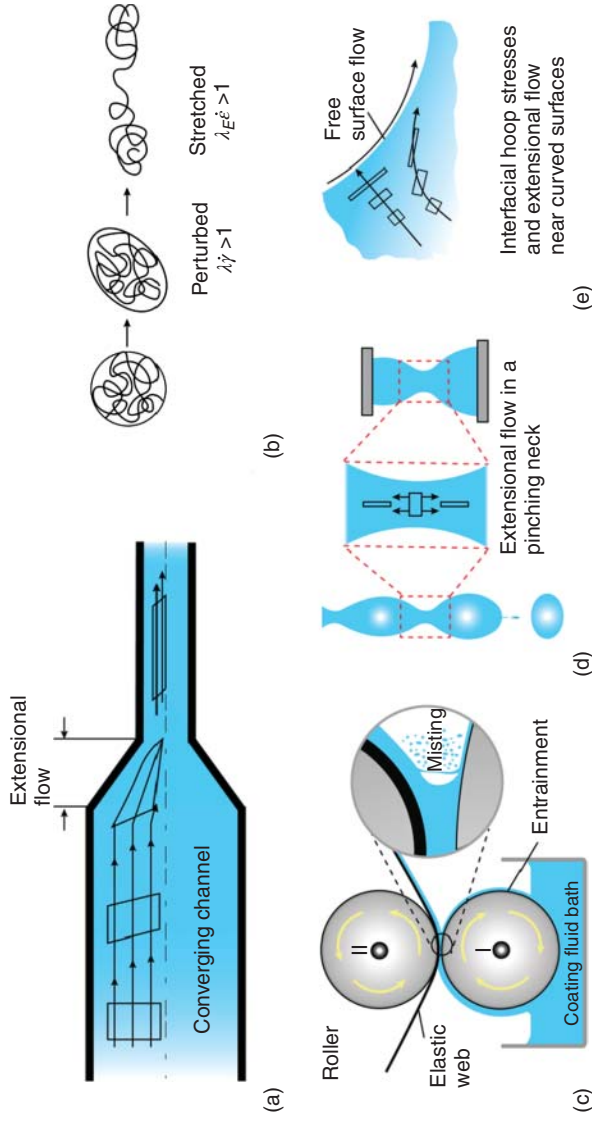
Jelena Dinic, Carina D. V. Martínez Narváez, and Vivek Sharma

Department of Chemical Engineering, University of Illinois at Chicago, Chicago, IL, USA

## 1 Introduction

Polymer rheology describes the response of macromolecular solutions and melts to applied deformation and flow. One of the longstanding and challenging goals of macromolecular engineering research is to identify and elucidate the influence of macromolecular parameters and interactions on macroscopic rheological behavior and processability [1–7]. Several excellent texts [1–3] and reviews [4–11] discuss substantial progress in identifying chemistry-independent universalities in shear rheology response of polymer solutions and melts at large length scales and time scales. Shear flows, associated with velocity gradients perpendicular to flow direction, arise within channels and near moving substrates. Most processing operations that aim at controlling flow rate or production rate rely on the measurement and control of shear viscosity,  $\eta$  that quantifies the resistance to shear flow. Extensional flows, associated with streamwise velocity gradients, arise in nearly all processing operations that involve expanding or contracting channels, stagnation points (in T-junctions and cross-slots), pinching necks formed during dripping and jetting, or curved free surfaces (in coating and printing operations), as sketched in Figure 1 [9–13, 19, 21–24]. Even though the Newtonian simple fluids display a rate-independent extensional viscosity,  $\eta_E = 3\eta$  that is three times the shear viscosity, the polymeric complex fluids show relatively large values. For example, dilute solutions of flexible polymers show extensional viscosity values  $10^3$ – $10^5$  times shear viscosity and display significant strain hardening. This massive extensional viscosity enhancement arises for high molecular weight flexible polymers due to a substantial increase in drag correlated with the dynamics of significantly stretched chains. However, due to extreme sensitivity to the entire deformation history and difficulty in reaching a steady extensional rate, the characterization of extensional rheology response is considered quite challenging and remains less well explored than shear rheometry [9–13, 19, 21–25].

Polymer solutions are considered dilute below a critical overlap concentration,  $c^* \approx M_w/N_A R_g^3$  calculated by equating the volume per coil to the size of an unperturbed chain at equilibrium [1–3, 10]. Here  $N_A$  is Avogadro's number,



**Figure 1** Extensional flows spontaneously arise in many processing operations. (a) Converging channels in extrusion, porous media, and microfluidics are associated with extensional flows, though shear flows also arise near walls [12–14]. (b) Macromolecular conformational changes in the presence of shear and extensional flows. Shear flows weakly perturb macromolecular coils. In contrast, strong extensional flow fields can unravel the chains, leading to a pronounced coil-stretch transition for flexible neutral polymers [8, 10, 15, 16]. (c) Forward roll coating involves the formation of a liquid sheet connecting fluid entrained by the moving elastic web and roller I. Capillary-driven instabilities and filament pinching results in undesirable drop formation or misting that affect process productivity [17, 18]. (d) Capillary-driven flow field arises when fluid elements approach a free surface [20]. The interplay of interfacial hoop stress and extensional rheology response influences instabilities in printing and coating flows.

and the radius of gyration or chain size  $R_g \propto M_w^\nu$  depends on molecular weight,  $M_w$ , and excluded volume (EV) interactions. Solvent quality determines the values of EV exponent:  $\nu = 0.5$  for  $\theta$ -solvent (ideal chains) to  $\nu = 0.588$  for good solvent (expanded coils). By definition, as interchain interactions do not influence the static and dynamic properties of dilute solutions, the polymer dynamics are typically described in the highly dilute limit ( $c \ll c^*$ ) using single chain models by accounting for chain flexibility, entropic resistance to stretching, solvent-mediated hydrodynamic interactions (HI), and EV interactions [1–4, 7, 10, 26]. Unperturbed polymer coils in solution interpenetrate for concentrations  $c > c^*$ . Since macromolecules overlap even in their quiescent state for  $c/c^* > 1$ , we refer to these as intrinsically semi-dilute solutions. The macromolecular dynamics in such semi-dilute polymer solutions [1–4] are relatively challenging to describe even under shear flow due to the influence of large concentration fluctuations as well as local concentration-dependent HI and EV interactions. Additional topological interactions arise above the entanglement concentration,  $c_e$ , transforming the macromolecular dynamics and measurable rheological properties [1–4, 11, 27–39]. In this article, we focus on unentangled polymer solutions with  $c < c_e$  (or the scaled concentration,  $c/c^* < c_e/c^*$ ).

The polymer solutions with  $c/c^* < 1$  that are considered dilute under quiescent conditions or in shear are referred to as effectively semi-dilute in many extensional rheology studies due to the increased degree of overlap and interchain interactions in stretched chains [26, 40–45]. Shear viscosity of polymer solutions and melts decreases with shear rates,  $\dot{\gamma}$  for shear Weissenberg number,  $Wi_s = \dot{\gamma}\lambda_s > 1$  or if  $\dot{\gamma}$  exceeds the shear relaxation rate,  $1/\lambda_s$  that is correlated to the longest relaxation time of the chains. Though shear flows only weakly perturb the chain dimensions (as sketched in Figure 1), strong extensional flows with Weissenberg number,  $Wi = \dot{\epsilon}\lambda_s > 1$  or if extension rate,  $\dot{\epsilon}$  exceeds the relaxation rate leads to coil-stretch transition [10, 15, 16, 26, 45–47]. Furthermore, the macromolecular strain accumulated under sustained  $Wi > 1$  flows stretch chains to their full, finite extensibility limit and even cause chain scission [48–51]. The progressive stretching and alignment of chains dramatically change the intrachain and interchain interactions, impacting both the magnitude and the concentration-dependent scaling of  $\eta_E$  and  $\lambda_E$ , that are often distinct from the corresponding  $\eta$  and  $\lambda_s$  values measured in response to viscometric shear flows [26, 27, 40, 43, 44, 52]. The influence of macromolecular parameters and interactions on the response to extensional flows remains relatively less well explored [7–10], partially due to the challenges involved in the description of the dynamics of stretched and orientated chains [7–12, 26, 32, 45, 53] and the well-documented challenges of extensional rheometry [9–13, 19, 21–25, 32].

We elucidate the influence of chemical structure (i.e., polymer choice) and resulting macromolecular parameters on pinching dynamics and extensional rheology response of aqueous polymer solutions. Even though many water-soluble polymers are used as rheology modifiers, the choice is primarily based on their shear rheology response. At relatively small concentration (typically  $< 1$  wt.%), polymers provide formulations with an enhanced zero shear viscosity (and are therefore called thickeners) and a well-defined shear thinning behavior [54–59]. Enhanced shear viscosity at low shear rates increases the

stability against flocculation or aggregation (and shelf life) and controls the spreading rate and area over a target substrate (e.g., skin for cosmetics, wall for paints, plates for food, or paper for inks). Likewise, adequate shear viscosity reduction facilitates mixing and pouring at intermediate shear rates ( $10^0 < \dot{\gamma} < 10^2 \text{ s}^{-1}$ ) and liquid transfer to substrates at higher rates ( $10^3 < \dot{\gamma} < 10^6 \text{ s}^{-1}$ ) [60–65]. However, shear rheology response is often found to be poorly correlated with processability and heuristic properties like stickiness, tackiness, stringiness, cohesiveness, jettability, printability, gloppiness, and spinnability [13, 19, 48, 66–69]. Such properties that depend on extensional rheology response are often determined qualitatively by examining the pinching behavior of a liquid neck or filament stretched between finger and thumb, or between a rod and reservoir, or by visualizing dripping/jetting behavior [13, 19, 38, 65, 67, 69]. However, quantitative assessment of such heuristic properties requires the understanding of interfacial flows and instabilities, as well as material properties underlying pinching dynamics [12, 13, 19, 23, 24, 36–44, 48, 56, 61, 62, 69–86]. In particular, characterizing and understanding extensional rheology response assumes a critical significance as stream-wise velocity gradients associated with extensional strain,  $\epsilon$  and extensional strain rates,  $\dot{\epsilon}$  spontaneously arise during capillarity-driven pinching of liquid filaments [13, 19, 48] and next to curved free surfaces in coating flows [20]. In this article, we introduce *capillarity-driven pinching* in lieu of the conventional term “capillary thinning and breakup” (or and pinch-off) to avoid confusion with (shear) thinning measured using capillary rheometers [60].

This contribution provides an overview of the key viscometric quantities that describe the shear and extensional rheology response of polymeric complex fluids and summarizes the methods and challenges for extensional rheology characterization. We focus on the analysis of capillarity-driven pinching of liquid necks that facilitates the measurement of the strain and strain-rate dependent extensional viscosity (also referred to as tensile growth coefficient),  $\eta_E = \eta_E^+(t, \dot{\epsilon})$ . As the measurement of steady values,  $\eta_E(\dot{\epsilon}) = \eta_E^+(t, \dot{\epsilon}); t \rightarrow \infty$  are relatively rare, often the plots show  $\eta_E = \eta_E^+(t, \dot{\epsilon})$  as a function of extensional strain,  $\epsilon$ . In many viscoelastic fluids, pinching dynamics displays elastocapillary (EC) dynamics, yielding an extensional relaxation time,  $\lambda_E$  that can be extracted from the decay constant of the exponential decrease in radius over time. Additionally, the value of steady, terminal extensional viscosity,  $\eta_E^\infty$  can be computed if a terminal viscoelastocapillary (TVEC) regime with a linear decrease in radius is manifested due to finite extensibility of polymer chains [12, 13, 18, 19, 23, 24, 36–44, 48, 56, 61, 62, 66, 69–119]. The extensional relaxation time,  $\lambda_E$  represents the time needed for chain relaxation after an extensional or stretching deformation, whereas  $\eta_E^\infty$  is correlated with extensibility [19, 26, 43, 45, 120]. Next, we define the macromolecular parameters required to describe the rheological response of polymer solutions (and melts), focusing on viscosity and relaxation time measured in response to shear and extensional flows. To keep the discussion focused but comprehensive, we limit the discussion to unentangled aqueous polymer solutions, supported by our experimental studies, made with dripping-onto-substrate (DoS) rheometry protocols we introduced in 2015 [36, 40–42, 77, 79].

We elucidate the influence of chemical structure (i.e., polymer choice) and resulting macromolecular parameters like flexibility (or persistence length) and

molecular-weight dependent extensibility on pinching dynamics and extensional rheology response of aqueous solutions of 2-hydroxyethyl cellulose (HEC) and poly(ethylene oxide) or PEO. Polysaccharides including HEC are often employed as rheology modifiers [54–59, 121] in inks, paints, and coatings [24, 39, 65, 122, 123], foods [38, 74, 82, 86, 121], pharmaceuticals [85], and cosmetics [61, 62, 83, 84, 122, 123], in preference to flexible polymers like PEO. Here we pursue the long-standing questions around their distinctive influence on flow behavior, processing, and performance of solutions and formulations. We describe how this pursuit involves intertwined quests and insights into fluid mechanics, nonlinear viscoelasticity, coil-stretch transition (and hysteresis), conformation-dependent hydrodynamic and EV interactions, and finite extensibility. We infer that the influence of chemistry can be evaluated *a priori*, using three macromolecular parameters: flexibility, extensibility, and segmental dissymmetry, defined and detailed herein. We anticipate that this critical progress and understanding of the influence of polymer concentration, solvent choice, and the three macromolecular parameters will inspire macromolecular engineering approaches toward developing materials and formulations with controlled flow behavior, determining optimal processing parameters, as well as for developing more realistic constitutive models to describe the response to imposed shear and extensional flow.

## 2 Background and Definitions: Polymer Physics, Pinching Dynamics, and Rheology

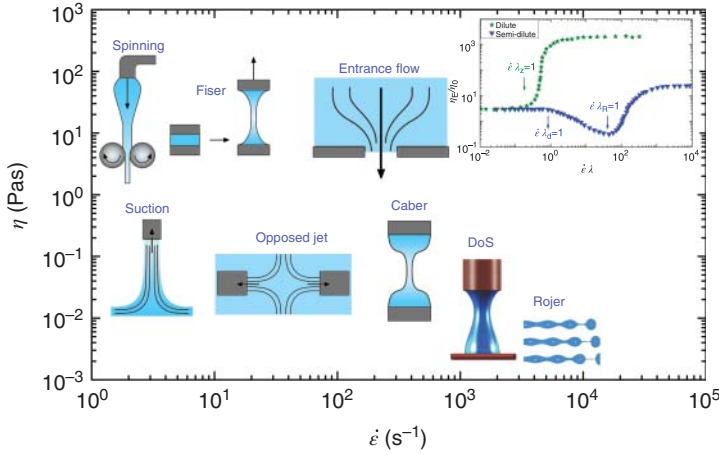
### 2.1 Shear and Extensional Rheology: Basic Concepts and Methods

The response of simple fluids to flow created by applied pressure gradients or by drag next to a moving surface can be analyzed using Newton's law of viscosity [1–3, 14, 15, 29, 60]. The constitutive equation states that the fluid stress,  $\tau$  increases linearly with the deformation rate,  $\dot{\gamma}$  and proportional to a rate-independent material-dependent property called shear viscosity,  $\eta$ . Simple fluids like water, glycerol, and organic solvents (like toluene) can be described using Newton's law of viscosity. Their extensional viscosity is three times larger than shear viscosity, implying only one constant parameter,  $\eta$  is needed for describing shear and extensional rheology of Newtonian fluids. However, comprehensive modeling and characterization of the rheological response of polymeric complex fluids require a description of four key phenomena that display non-Newtonian behavior and related rheological measures [60, 124]. (i) Rate-dependent viscosity,  $\eta(\dot{\gamma})$ , for solutions and melts of linear polymers often exhibit shear thinning, that is, steady shear viscosity decreases with increase in shear rate,  $\dot{\gamma}$ . The rate-dependent variation in viscosity can be described using Generalized Newtonian fluid models, including the two-parameter power-law model described by  $\tau = K\dot{\gamma}^n$  or  $\eta(\dot{\gamma}) = K\dot{\gamma}^{n-1}$  that includes a prefactor called consistency,  $K$  and a power-law index,  $n < 1$  [60, 125]. (ii) Stress relaxation, captured by time-dependent modulus  $G(t; \lambda)$  describes the time-dependent variation in stress after step strain, and often the longtime response involves an

exponential decay, governed by the longest relaxation time,  $\lambda$  [1, 2, 29, 124, 126]. (iii) Normal stress differences  $N_1$  and  $N_2$  that drive rod climbing phenomena or the “Weissenberg effect” and contribute to elastic instabilities, especially in strong flows that involve curved streamlines [127–134]. (iv) Strain hardening in response to extensional flow, responsible for tubeless siphon, enhanced pressure drops in porous media flows, stringiness and spinnability of polymer solutions and melts, and the delayed pinch-off of viscoelastic fluid filaments [9–13, 19, 21–25, 32, 36, 37, 39–44, 76–81, 112, 118, 119, 135–138].

Deformations and recovery of elastic polymeric fluids in the limit of small deformations, known as a linear viscoelastic response, can be captured by using the simplest models for macromolecular dynamics that consider polymer chains as elastic dumbbells: two Stokes beads (capture drag) connected by a Hookean spring (entropic elasticity) [29]. The elastic dumbbell model is the molecular basis for the upper-convected Maxwell model and the Oldroyd-B model [29]. Bead-spring models including Rouse and Zimm models, discussed in the next section, include a large number of beads (number increases in proportion to molecular weight) and thus incorporate a spectrum of relaxation times [1, 2, 29, 60, 124, 126, 139–141]. However, the response to large deformations or non-linear viscoelastic response requires additional considerations: non-Hookean elastic response, finite extensibility, and conformation-dependent drag [7, 26, 29, 45, 142, 143]. The advent of advanced torsional rheometers, in particular, has facilitated the characterization of the steady and unsteady response to shear flows [60]. The utility and limitations of different geometries and test profiles available for torsional rheometry characterization and other measurement techniques available for measuring shear rheology response are summarized by Macosko, among others [60, 125, 126].

However, characterizing extensional rheology response is rather challenging as measurements require bespoke instrumentation, display high sensitivity to deformation history, and are susceptible to elastic or inertial flow instabilities that can arise in microfluidic and stagnation flow devices [12, 13, 19, 23–25, 36, 144]. Most techniques, especially fiber spinning techniques and FISER (filament stretching rheometry), are suitable for polymer solutions with relatively high viscosity, and typically the range of accessible strain or strain rates is somewhat limited, as shown in Figure 2 [11, 23–25, 60, 118, 135, 136, 145]. Bulk, macroscopic measurements carried out by measuring stress required to stretch liquid bridges at the constant extensional rate in FISER are reviewed in McKinley and Sridhar [118], and the focus of more recent papers on entangled polymer solutions and melts [11, 21, 32, 53, 146–148], whereas McKinley (2005) presents a comprehensive summary of extensional rheology characterization based on capillarity-driven pinching flows including CaBER (capillary breakup rheometry). Dontula et al. showed that strong inertial and shear within the nozzle effects render the opposed jets technique unsuitable for quantitative or accurate measurements of  $\eta_E$  [149, 150]. It is well-established that the extensional rheology response exhibits a high sensitivity to deformation history, revealing distinct behavior based on the experimental protocol used [12, 23, 96, 151, 152]. Therefore, the analysis of pinching dynamics provides access to extensional rheology response at strain rates most relevant for liquid transfer applications.




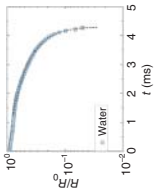

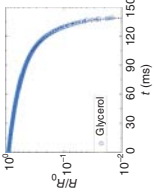

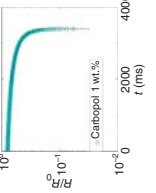

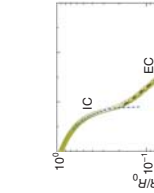

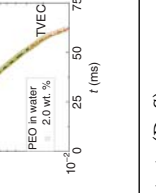
**Figure 2** Most standard techniques are used for characterizing the extensional rheology response of polymeric solutions. The range of zero shear viscosity (on the y-axis), and the extension rates (on the x-axis) constrained by the design limitations determine the suitability of each technique. The inset shows the typical scaled extensional viscosity response (or Trouton ratio) as a function of dimensionless extension rate (or Weissenberg number) for dilute polymer solutions [103] and semi-dilute, entangled polymer solutions [21].

## 2.2 Capillarity-driven Pinching Dynamics

Table 1 summarizes and lists the typical neck shapes and radius evolution profiles associated with capillarity-driven pinching flows of Newtonian and non-Newtonian fluids. The local balance of capillarity, inertial, and viscous stresses determines the pinching dynamics for Newtonian fluids [70, 71, 73]. Additional contributions from rate-dependent viscosity and elastic stresses impact the pinching dynamics for many complex fluids [19, 36, 73, 77]. Low viscosity Newtonian solvents like water exhibit a single conical neck, and radius evolution displays inertio-capillary (IC) response [71, 78, 153, 154, 157]. In contrast, higher viscosity Newtonian fluids like glycerol exhibit a slender, cylindrical neck that exhibits visco-capillary (VC) pinching dynamics if Ohnesorge number,  $Oh = t_{VC}/t_R > 1$  [78, 155–157]. Here  $Oh = \eta/\sqrt{\rho\sigma R_0}$  represents a dimensionless viscosity for a fluid with viscosity,  $\eta$  density,  $\rho$  and surface tension,  $\sigma$ . Non-Newtonian formulations that show strong shear thinning response exhibit power law as pinching behavior and the neck pinches by forming two cones for power-law index,  $n < 0.66$ , whereas for  $n > 0.66$ , pinching of slender, cylindrical necks is observed [19, 77, 158–160, 162–164].

The addition of long, flexible polymers leads to extra viscoelastic stresses, that slow down pinching, and delay the pinch-off event, typically due to EC response, manifested with an exponential decay in radius. A detailed discussion of pinching dynamics, as anticipated by different constituent models for non-Newtonian fluids, can be found in many papers and reviews, especially those contributed by Entov [90, 91, 120, 161], Yarin [48, 88, 89, 161], Renardy [158, 162–164], McKinley, Rothstein, and Clasen [19, 24, 25, 43, 44, 52, 75, 80, 81, 95–98,

**Table 1 Capillarity-driven pinching dynamics:** The expressions derived from force balance in pinching neck, characteristic timescales, the relevant dimensionless groups for Newtonian and non-Newtonian fluids, and the expressions that can describe pinching dynamics (including viscoelastic EC or TVEC), respectively, are included together with selected references.

<p><i>Newtonian</i> Low viscosity <i>Inertio-capillary (IC)</i></p>		$\frac{R(t)}{R_0} = X \left( \frac{\sigma}{\rho R_0^2} \right)^{1/3} (t_f - t)^{2/3}$ $X = 0.4 - 0.8$	$t_R = (\rho R_0^3 / \sigma)^{1/2}$ $\text{Oh} < 1 \text{ Wi} = 0$ $\text{Ec} = 0$	
<p>Chen and Steen [153], Day et al. [154], Eggers and Fontelos [71], and Dinic and Sharma [78]</p>				
<p><i>Newtonian</i> High viscosity <i>Visco-capillary (VC)</i></p>		$\frac{R(t)}{R_0} = \frac{(2X-1)}{6} \frac{\sigma}{\eta R_0} (t_f - t)$ $X = 0.5324 - 1$	$t_{VC} = \eta R_0 / \sigma$ $\text{Oh} > 1 \text{ Wi} = 0$ $\text{Ec} = 0$	
<p>Papageorgiou [155], McKinley and Tripathi [156], and Castrejón-Pita et al. [157]</p>				
<p><i>Non-Newtonian</i> Shear thinning <i>Power law (PL)</i></p>		$\frac{R(t)}{R_0} = Y (t_f - t)^{\eta_e}$	$t_{PL} = Y^{-1/\eta_e}$ $\text{Oh} > 1$	
<p>Renardy [158], Doshi and Basaran [159], McKinley [19], Suryo and Basaran [160], and Dinic et al. [77]</p>				
<p><i>Non-Newtonian</i> Viscoelastic (VE) <i>Elasto-capillary (EC)</i></p>		$\frac{R(t)}{R_0} \approx \left( \frac{G_E R_0}{2\sigma} \right)^{1/3} \exp \left( -\frac{t-t_f}{3\lambda_E} \right)$	$\lambda_E$ $\text{VOh Wi} = 2/3$ $\text{De} > 1 \text{ Ec} > 0$	
<p>Entov and Yarín [161], Yarín [48], McKinley [19], Clasen et al. [44], and Dinic and Sharma [79]</p>				
<p><i>Non-Newtonian</i> Finitely extensible VE <i>Terminal ViscoEC (TVEC)</i></p>		$\frac{R(t)}{R_0} = \frac{\sigma}{2R_0 \eta_E^\infty} (t_f - t)$	$t_{TVEC} = 2R_0 \eta_E^\infty / \sigma$ $\text{VOh Wi} > 1$ $\text{De} > 1 \text{ Ec} > 0$	
<p>Renardy [162–164], Entov and Hinch [120], Stelter et al. [88, 89], Fontelos and Li [165], and Dinic &amp; Sharma [79]</p>				

The snapshots showing the characteristic neck shape and the radius evolution profiles were obtained by the coauthors using dripping-onto-substrate (DoS) rheometry [39].



103, 112, 114, 156, 166–174], and the coauthors [24, 36–42, 61, 62, 75–79, 95, 114, 119, 137, 138]. The modified expression listed in Table 1 (introduced by Dinic and Sharma [79]), allows accounting for the onset of EC at  $t_c$ , and the computation of the extensional relaxation time,  $\lambda_E$  as well as an apparent extensional modulus,  $G_E$  [40–42, 77, 79] as distinct from the corresponding values obtained from shear rheology characterization. Finite extensibility effects [79, 88, 89, 120, 165] can sometimes result in a terminal visco-elastocapillary (TVEC) response with  $R(t) \propto (t_f - t)/t_{TVEC}$ , yielding the measurements of the steady, terminal extensional viscosity  $\eta_E^\infty$  and the filament lifespan,  $t_f$  (or the overall pinch-off time). As  $t_{TVEC}/t_{VC} = \text{Tr}^\infty/3$ , we define  $\text{Tr}^\infty = \eta_E^\infty/\eta_0$  to be the terminal Trouton ratio that depends on the ratio of the mean squared size of stretched and unperturbed chains.

The dilute solutions of HEC and PEO with nearly matched measured shear viscosity and (estimated) relaxation time are expected to show matched response in the Newtonian and the EC regime based on the Entov–Hinch model (and its variants) [19, 44, 88, 89, 166, 175], with a contrast in the pinching dynamics anticipated only in the TVEC regime due to distinct values of  $\eta_E^\infty$ . The published literature lacks such close, quantitative comparisons, and we recently showed that these expectations are not realized in practice for reasons discussed and revisited herein [42]. The lack of such data and comparisons was partially due to the challenges involved in the characterization of capillarity-driven pinching of a filament created by applying step-strain to a fluid confined between two plates [19, 25, 52, 87–91, 103, 169, 176], likewise in the commercially available technique called CaBER. Four significant issues arise: (i) Pinch-off occurs before plate separation even with rapid step-strain for low viscosity ( $\eta < 50$  mPa·s), or low elasticity ( $\lambda_s, \lambda_E < 1$  ms) fluids [25]. (ii) The IC/VC-EC transition is not visualized (or gets masked) for unentangled polymer solutions [44, 79]. The EC regime for the semi-dilute solutions is neither easy to define nor fit [177]. (iii) The TVEC (or finite extensibility) regime, as well as the EC-TVEC transition, is typically not captured [79]. (iv) The extensional relaxation time,  $\lambda_E = \lambda_{EC} > \lambda_s$  obtained from the EC fit is greater in magnitude and exhibits a stronger concentration-dependence than the longest shear relaxation time,  $\lambda_s$  for unentangled flexible polymer solutions like PEO [44, 176]. The slow retraction method (SRM) avoids the fast stretch of the conventional CaBER technique [169], but then the self-thinning process might not drive or govern IC/VC-EC transition. We have established that the DoS rheometry protocols help overcome the first three characterization challenges [37, 38, 40, 41, 77, 79], and made progress toward understanding the concentration-dependent scaling of the extensional rheology response by a careful assessment of stretched polymer physics.

Here, we characterize the pinching dynamics and extensional rheology response using DoS rheometry protocols [36–38, 40–42, 77, 79]. Several studies, including our own, describe the characterization of the extensional rheology and pinching dynamics using (DoS) rheometry for solutions of neutral and charged polymers [36–41, 77, 79, 119, 137, 138, 178–184], inks and particle suspensions [77, 172, 174], wormlike micellar solutions [77, 185–188], hydrocolloids and food materials (cellulose gum solutions, ketchup, mayo) [38, 77], and cosmetics (nail lacquer formulations, hand-cream, shampoo, and conditioners) [61, 62, 77].

The DoS rheometry involves visualization and analysis of pinching necks created by dripping a finite volume of a liquid from a fixed nozzle onto a partially wetting substrate. Briefly, the fluid is pumped at a low and fixed flowrate,  $Q = 0.02 \text{ ml min}^{-1}$ , through a nozzle with an outer and inner diameter of  $D_o = 2R_o = 1.27 \text{ mm}$  and  $D_i = 0.838 \text{ mm}$ , respectively. A finite volume of the liquid is released onto a substrate placed at distance  $H$ , such that the aspect ratio of  $H/D_o \approx 3$ . The DoS videos are further analyzed with specially written MATLAB codes for determining radius evolution over time. The specific challenges that arise for HEC solutions due to extremely short-lived EC and TVEC regimes in unentangled and entangled solutions are detailed elsewhere [189]. Here, we focus on revisiting the HEC versus PEO comparison.

### 2.3 Polymer Dynamics in Unentangled Solutions: Rouse, Zimm, and Rouse–Zimm Chains

For dilute solutions, the macromolecular dynamics in quiescent conditions (dynamic light scattering) and shear flow for dilute solutions are captured quite well by Zimm model [1, 2, 10, 141], a single chain model that accounts for both EV and HI. In contrast, the original Rouse model [2, 10, 140] that neglects both effects (and is inconsistent with the measured response of dilute solutions) is found to describe the dynamics of unentangled melts quite well. The Rouse and Zimm models in their original form are bead-spring models and allow an estimate of relaxation time using the formula,  $\lambda_s = R^2 \zeta / k_B T$  (ignoring the prefactors obtained by the exact calculations). Here,  $R$  represents the root mean squared ensemble-averaged coil size that equals the unstretched length,  $R_{us} = \langle R_o \rangle^{1/2} = N_K^{1/2} b_K$ . The relaxation time is set by diffusion coefficient ( $D = k_B T / \zeta$  or the ratio of thermal energy to friction coefficient), and  $N_K$  and  $b_K$  are the respective number of Kuhn segments and Kuhn length. In the Rouse model,  $\zeta \propto M$  or increases linearly with molecular weight, whereas in the Zimm model, as  $\zeta \propto R \propto M^\nu$ , the drag coefficient has lower magnitude (due to HI). Both Rouse time,  $\lambda_R \approx \lambda_o N_K^2$  and Zimm time,  $\lambda_Z \approx \lambda_o N_K^{3\nu}$  depend on the same monomer relaxation time,  $\lambda_o \approx \eta_s b_K^3 / k_B T$ , where  $\eta_s$  refers to the solvent viscosity. The progressive screening of both EV and HI in intrinsically semi-dilute solutions can be captured to a good approximation using the composite Rouse–Zimm model or the blob models [1, 3].

The blob theory, as originally devised for intrinsically semi-dilute solutions, assumes that on length scales larger than the correlation length ( $\xi_h \approx \xi$ , hydrodynamic comparable to EV screening length), the dynamics are many-chain-like Rouse-like dynamics are followed with both EV and HI screened. The time scale associated with the blob relaxation is determined by utilizing the Zimm model,  $\lambda_\xi \approx \eta_s \xi^3 / k_B T$ . The number of monomers in the correlation blob is  $g \approx \phi \left( \frac{\xi}{b} \right)^3 \approx \phi^{-1/(3\nu-1)}$  and the volume fraction  $\phi$  is related to the concentration  $c'$  in mass/volume by the expression  $\phi = c' N_K b_K^3 N_A / M_w$ . The Rouse–Zimm model then captures the relaxation time for a chain of blobs as described by the following equation:

$$\lambda_{RZ} \approx \lambda_\xi (N_K^2 / g^2) \approx \lambda_o N_K^2 \phi^m \quad (1)$$

The exponent that describes concentration dependence is  $m = (2 - 3\nu)/(3\nu - 1) \cong 0.31$  for good solvents (EV interactions included) and  $m = (2 - 3\nu)/(3\nu - 1) \cong 1$  if EV interactions are screened or absent.

In the 1970s, de Gennes and Pincus postulated that the single polymer chains under tension could be described by considering an equivalent chain made up of tension blobs [3, 190, 191] (or Pincus blobs), such that structural anisotropy and the influence of the applied tension on intrachain interactions play a role only above  $\xi_t$ . At the molecular level, the question that remains unanswered is how such a chain of Pincus blobs relaxes or behaves when surrounded by a sea of similarly stretched chains in a good solvent. Recently, Prabhakar et al. [26, 45] proposed a constitutive model for unentangled polymer solutions in a theta solvent by combining the tension blob and conformation-dependent drag frameworks and inferred that stretching strengthens intermolecular interactions in the dilute regime but weakens those in the semi-dilute regime. However, Prabhakar et al. [26] acknowledged the need for similar models for stretched chains in a good solvent, and the utter lack of extensional rheology data for the intrinsically semi-dilute, unentangled solutions. This article revisits the extensional relaxation time data we acquired for intrinsically semi-dilute, unentangled solutions in a good solvent ( $1 < c/c^* < c_e/c^*$ ) and summarizes our findings on the influence of solvent and polymer properties.

The polymer contribution to shear viscosity for dilute and semi-dilute unentangled solutions can be estimated using  $\eta_p \approx G\lambda$ , with  $G \approx \phi k_B T / N_K b_K^3$  and in semi-dilute unentangled solutions, this yields,  $\eta_p \propto \eta_s \phi^{m+1}$ , with stronger dependence than the linear law,  $\eta_p \propto \phi^1$  obtained for the dilute regime. It is more common to describe the concentration-dependent increase in specific viscosity,  $\eta_{sp} = \eta_p / \eta_s$  in terms of the degree of overlap or as  $\eta_{sp} = (c/c^*)^{m+1} = (c/c^*)^{1/(3\nu-1)}$ . Experiments show that above entanglement concentration,  $c_e$ , the behavior changes to much stronger concentration dependence  $\eta_{sp} = (c/c^*)^{3/(3\nu-1)}$  due to the role played by topological interactions (or entanglements). The plot of zero shear viscosity (determined from rate-independent viscosity at low shear rates) against molecular weight for polymer melts, also known as the Berry-Fox plot, a transition from a linear scaling of  $\eta_0 \propto M$  to stronger than cubic dependence,  $\eta_0 \propto M^{3.4}$  occurs beyond the entanglement molecular weight,  $M_e$ . The textbook by Dealy et al. surveys the current state-of-the-art in polymer melt rheology [139]. Fairly extensive literature focuses on the shear and extensional rheology response of entangled melts, as the application and processing of commodity plastics require both understanding and control over their shear and extensional rheology [11, 21, 26–29, 31–36, 45, 53, 146–148, 192, 193]. Several studies [112, 114, 194–196] detail the role of entanglements in promoting spinnability, a heuristic property, often correlated with the successful production of continuous filaments using either conventional (dry, wet, dry-jet, and gel spinning) [197] or emerging methods (electrospinning, centrifugal force spinning, and blow spinning) [113, 195, 198–202]. Correspondingly, unentangled solutions are considered suitable for applications where drop formation is desired, and stringiness, as well as long-lived fluid threads, pose processing challenges.

## 2.4 Macromolecular Flexibility, Extensibility, and Segmental Dissymmetry

The contrast in local flexibility or stiffness scales with the magnitude of Kuhn length,  $b_K$ , or persistence length,  $l_p = b_K/2$  as  $l_p$  is the characteristic length scale correlated with an exponential decay in angular correlations along a chain backbone [1–3, 5, 6]. Polymers can be classified as globally flexible, semi-flexible, or rigid-rods [1, 2, 8, 203, 204] by comparing the Kuhn length,  $b_K$  to the contour length,  $R_{\max} = N_K b_K$  or based on their ratio,  $N_K = R_{\max}/b_K$ . Biomacromolecules like DNA, actin, collagen, polysaccharides, and synthetic polymers like poly(benzyl glutamate) and Kevlar are often considered semi-flexible [1, 2, 8, 203–206] due to the relatively large values of  $l_p$ . Semi-flexibility influences both thermodynamic and hydrodynamic properties [1–3, 8, 203–209]. Here, we consider polysaccharides to be *semi-flexible chains* recognizing that their static and dynamic behavior is distinct from the behavior exhibited by *semi-flexible filaments* like actin, collagen, carbon nanotubes, and fd-virus; for the latter, contour length is comparable to persistence length or  $N_K \sim O(10)$  (or lower) [173, 206, 210]. Extensional viscosity of FENE-P chains (finitely extensible nonlinear elastic, with Peterlin's preaveraging approximation) in ultra-dilute solutions can be written as  $\eta_E^\infty \rightarrow 3\eta_s + 2\eta_p L_E^2$  exhibiting a dependence on both polymer contribution to shear viscosity,  $\eta_p$  as well as the finite extensibility parameter,  $L_E^2 = (R_{\max}/R_{us})^2 = N_K^{2(1-\nu)}$ , defined as the ratio of the contour length of a chain,  $R_{\max} = N_K b_K$  to the unstretched length,  $R_{us} = \langle R_0 \rangle^{1/2} = N_K^\nu b_K$ . Thus in addition to  $N_K$ , the finite extensibility parameter depends on the polymer–solvent interactions (including the EV interactions) [19] that determine the value of the solvent quality exponent,  $\nu$ .

In the 1970s, deGennes [3, 15], Tanner [211], and Hinch [212] discussed that chains undergo coil-stretch transition beyond a critical extension rate,  $\dot{\epsilon}_{C \rightarrow S}$  and due to coil-stretch hysteresis, the prestretched chains relax back by undergoing stretch-coil transition,  $\dot{\epsilon}_{S \rightarrow C} < \dot{\epsilon}_{C \rightarrow S}$  at a lower rate implying that the stretched state of polymers can be maintained if deformation rate stays above  $\dot{\epsilon}_{S \rightarrow C}$ . The physical reality of coil-stretch hysteresis remained under scrutiny [211–214] until DNA-based microfluidics experiments by Schroeder et al. [16, 215], showed both transition and hysteresis. Furthermore, simulations by Schroeder et al. [16, 215], and by Hsieh and Larson [216–218] demonstrated that coil-stretch hysteresis manifests itself if  $\zeta_s/\zeta_c > 4.5$  or the ratio of drag coefficients of stretched to unperturbed coils exceeds a critical value of 4.5. Schroeder et al. [8, 9, 16, 215] reported direct observation of coil-stretch transition and hysteresis of fluorescently labeled longer bacterial genomic DNA ( $R_{\max} = 1300 \mu\text{m}$ ) with a drag ratio of 5 and absence of hysteresis for  $\lambda$ -DNA ( $R_{\max} = 20 \mu\text{m}$ ) with a drag ratio of 1.6. The coil-stretch transition takes place beyond the critical extensional rate  $Wi = \lambda_s \dot{\epsilon}_c > 1/2$  defined by a concentration-dependent shear relaxation time. The drag coefficient for spherical coil,  $\zeta_c$  based on Zimm model, and  $\zeta_s$  for stretched chains based on the rigid rod are given as:

$$\zeta_c = (3/8)(6\pi^3)^{1/2} \eta_s R_c = 5.11 \eta_s R_c \quad (2a)$$

$$\zeta_s = \frac{6.28\eta_s R_{\max}}{\ln(R_{\max}/d)} = \frac{6.28\eta_s N_K b_K}{\ln(N_K b_K/d)} \quad (2b)$$

The ratio of drag coefficients of the stretched to the coiled chain is given by the following expression:

$$\zeta_s/\zeta_c \approx R_{\max}/R_c \ln(N_K b_K/d) \approx L_E/\ln(N_K b_K/d) \quad (3)$$

The calculation of coil-stretch transition and hysteresis criteria using the ratio of drag coefficients requires the value of an additional length-scale,  $d$  that represents the hydrodynamic diameter of a Kuhn segment. Even though the Kuhn length,  $b_K$  can be obtained from experiments or theory, the hydrodynamic diameter,  $d$  is not usually specified or measured for most polymers. According to Larson [124], the actual diameter of the Kuhn segment can be estimated using  $d_K^2 l = 4M_0/0.82j\pi N_A \rho$  by matching the volume occupied by  $N_K$  Kuhn segments of a chain with the volume per coil in a melt. The formula uses the molecular weight of a chemical monomer  $M_0$  and bond length,  $l$  and assumes  $j$  is equal to the number of monomeric carbon atoms in the polymer backbone ( $j=2$  for polymers like PS or PE), and the factor 0.82 accounts for the tetrahedral bond angle. However, the relationship between  $d$  and  $d_K$  is not obvious.

We posit that a practically more suitable and rheologically relevant alternative for computing  $d$  is the use of packing length,  $p = (\pi/4)d_K^2/b_K \approx d^2/b_K$ . Fetters et al. [30, 192, 193, 219] have shown that for flexible polymers like PEO, the plateau modulus,  $G_e$ , the entanglement molecular weight,  $M_e$ , or the tube length,  $a$  can all be defined in terms of a packing length,  $p$ . Witten et al. [220] identified  $p$  as the length scale that provides a measure of polymer elasticity. Dividing the Kuhn segment size (a measure of local flexibility) with the packing length, correlated with the entanglement modulus (the macroscopic measure of elasticity), we obtain a new dimensionless measure we define as segmental dissymmetry:

$$S_d = \frac{b_K}{p} \approx \frac{b_K^2}{d^2} \quad (4)$$

The segmental dissymmetry,  $S_d$  values estimated using data provided in Fetters et al. [30, 193, 219] range from 2.5 to 4.5 for flexible polymers. The criteria for coil-stretch hysteresis can be effectively rewritten as

$$\zeta_s/\zeta_c \approx L_E/\ln(N_K S_d^{0.5}) \quad (5)$$

in terms of flexibility, extensibility, and segmental dissymmetry. Thus, coil-stretch transitions are most likely to occur for polymers with small segmental dissymmetry and large extensibility. Since the value of  $S_d$  is directly correlated with segmental shape and size, its value determines the criteria for the coil-stretch transition and affects the propensity to form liquid crystalline phases [2, 205]. By identifying the central role of  $S_d$  (segmental dissymmetry), defined in terms of packing length,  $p$  in determining coil-stretch hysteresis, we make a formal connection between the macromolecular parameters needed to describe the stretched chain hydrodynamics in dilute solution with the chain dynamics in entangled solutions and melts.

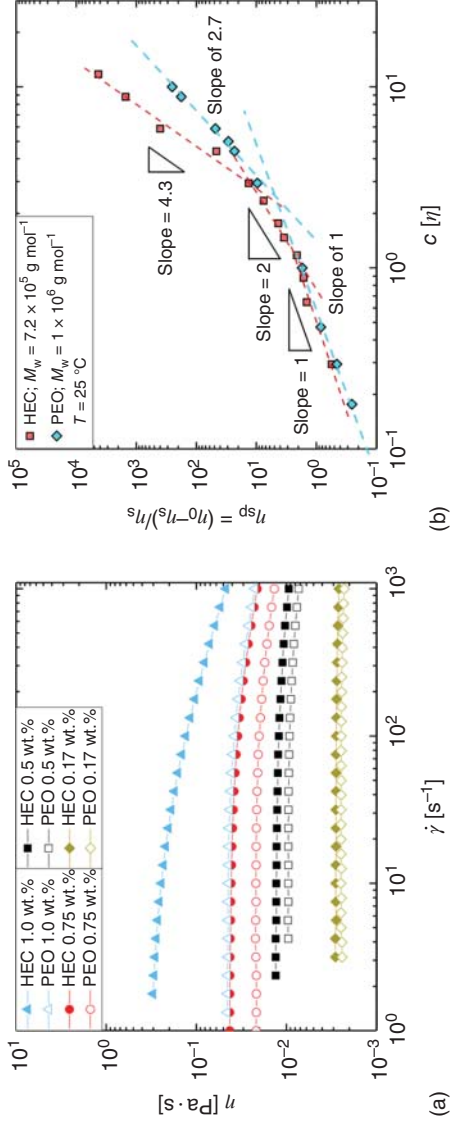
The value of  $S_d$  can be determined from rheological measurements and empirical correlations established in the literature for entangled polymers [30, 192, 193, 219–221]. For example, the number of entanglement strands,  $P_e$  in the volume equal to the cube of tube diameter (or  $a = N_e^{1/2} b_K$ ) is given by  $P_e = a/p$ . For flexible polymers, seemingly chemistry-independent constant values of  $P_e \approx 20$  is observed. Thus, the  $S_d$  value can be computed to be  $S_d = P_e/N_e^{1/2} \approx 20/N_e^{1/2}$  for flexible polymers, showing a direct connection of segmental entanglement molecular weight,  $M_e$ .

The entanglement molecular weights of polysaccharides are hard to measure as polysaccharide melts cannot be prepared, and reliable measurement of the plateau modulus of entangled polysaccharide solutions is also challenging. However, recently Horinaka et al. [222, 223] computed the  $M_e$  and  $P_e$  values for several polysaccharides by utilizing rheological measurements in ionic liquids and determined  $P_e$  of 40 for amylose, 72 for carboxymethylcellulose (CMC), and 220 for cellulose, respectively. We hereby conjecture that the contrast between flexible and semi-flexible polymers observed in terms of entanglement concentration (or the response to shear flow), pinching dynamics, the values of  $P_e$ , and the response to an extensional flow field, all appear to be correlated with the relatively high  $S_d$  of polysaccharides.

### 3 Influence of Three Macromolecular Properties on Rheological Response

#### 3.1 Contrasting Steady Shear Viscosity Measurements for Aqueous HEC and PEO Solutions

Shear viscosity measurements, as a function of shear rate obtained for a range of concentrations of aqueous solutions of HEC and PEO using a torsional rheometer, are shown in Figure 3a. A concentration-dependent increase in viscosity can be observed for both polymers. However, the zero-shear viscosity,  $\eta_0$  values show a stronger increase for HEC than for PEO solutions, even though  $\eta_0$  values are comparable at matched concentrations below  $c = 0.17$  wt.%. Figure 3b contrasts the polymer contribution to solution viscosity in terms of computed specific viscosity  $\eta_{sp} = (\eta_0 - \eta_s)/\eta_s$ . At the critical overlap concentration,  $c^* \approx 0.17$  wt.%,  $\eta_{sp} = 1$  and the solution viscosity is twice the solvent viscosity,  $\eta_s = 0.9$  mPa·s. Both overlap concentration and intrinsic viscosity,  $[\eta] = 1/c^* = 5.98$  dl g<sup>-1</sup> obtained for the aqueous HEC solutions, match the values obtained for the aqueous PEO solutions, implying that both polymeric systems utilized in this study at matched concentrations exhibit matched values of overlap parameter,  $c/c^*$  or Berry number,  $c[\eta]$ . Therefore, dilute solutions of both polymers that have matched the value of  $c/c^*$  or  $c[\eta]$  appear indistinguishable in shear, as shown in Figure 3a. Although the nondilute solutions ( $c[\eta] > 1$ ) of both HEC and PEO exhibit shear thinning, the HEC solutions show higher zero shear viscosity values, a higher degree of shear thinning, and exhibit a stronger concentration-dependent increase in specific viscosity at matched  $c[\eta]$  values.



**Figure 3** Shear rheology of the aqueous HEC and PEO solutions. (a) Steady shear viscosity measurements for aqueous HEC solutions are contrasted against the measured response of aqueous PEO solutions. The comparison reveals a stronger concentration-dependent increase in viscosity and a higher extent of shear thinning for the HEC solutions. (b) Specific viscosity data as a function of concentration show three distinct regimes for the HEC solutions (i) dilute below overlap concentration,  $c^* = 0.17$  wt.% (ii) semi-dilute, unentangled ( $c^* < c < c_e$ ), and (iii) semi-dilute entangled above entanglement concentration,  $c_e > 0.5$  wt.%. In contrast, for the aqueous PEO solutions, the observed behavior can be classified as dilute below  $c^* = 0.17$  wt.% and semi-dilute, unentangled for all PEO concentrations with  $c > c^*$ . The shear rheology response of the polymer solutions was characterized using a concentric cylinder (double gap) Couette cell for low viscosity aqueous HEC and PEO solutions ( $\eta_0 < 0.2$  Pa·s) and cone-and-plate geometry (50 mm diameter,  $1^\circ$  cone) for higher viscosity solutions on an Anton Paar MCR 302 rheometer (torque range  $10^{-5}$ –200 mN·m) at  $25^\circ\text{C}$ .

Specific viscosity of HEC solutions exhibits three distinct scaling regimes:  $\eta_{sp} \propto c$  in dilute ( $c < c^*$ ),  $\eta_{sp} \propto c^2$  in the semi-dilute, unentangled ( $c^* < c < c_e$ ), and  $\eta_{sp} \propto c^{4.3}$  in the entangled ( $c > c_e$ ) regime. The scaling exponent in the semi, dilute entangled regime (4.3, as  $\eta_{sp} \sim c^{4.3}$ ) agrees well with the value  $\eta_{sp} \sim c^{4.2}$  for  $c > c_e$  reported by Del Giudice et al. [224]. In contrast, the specific viscosity data for aqueous PEO solutions (see Figure 3b) exhibit only two regimes:  $\eta_{sp} \propto c$  ( $c < c^*$ ), and  $\eta_{sp} \propto c^{2.7}$  for unentangled, semi-dilute ( $c^* < c < c_e$ ) solutions. The entangled regime for flexible polymers [1] typically lies beyond  $c_e/c^* \approx 5-10$  and is beyond the range for PEO concentrations investigated herein. In contrast, for aqueous HEC solutions, the entangled regime with a stronger concentration dependence emerges beyond  $c_e = 0.5$  wt.% (corresponds to  $c_e/c^* \approx 3$ ), as shown in Figure 3b.

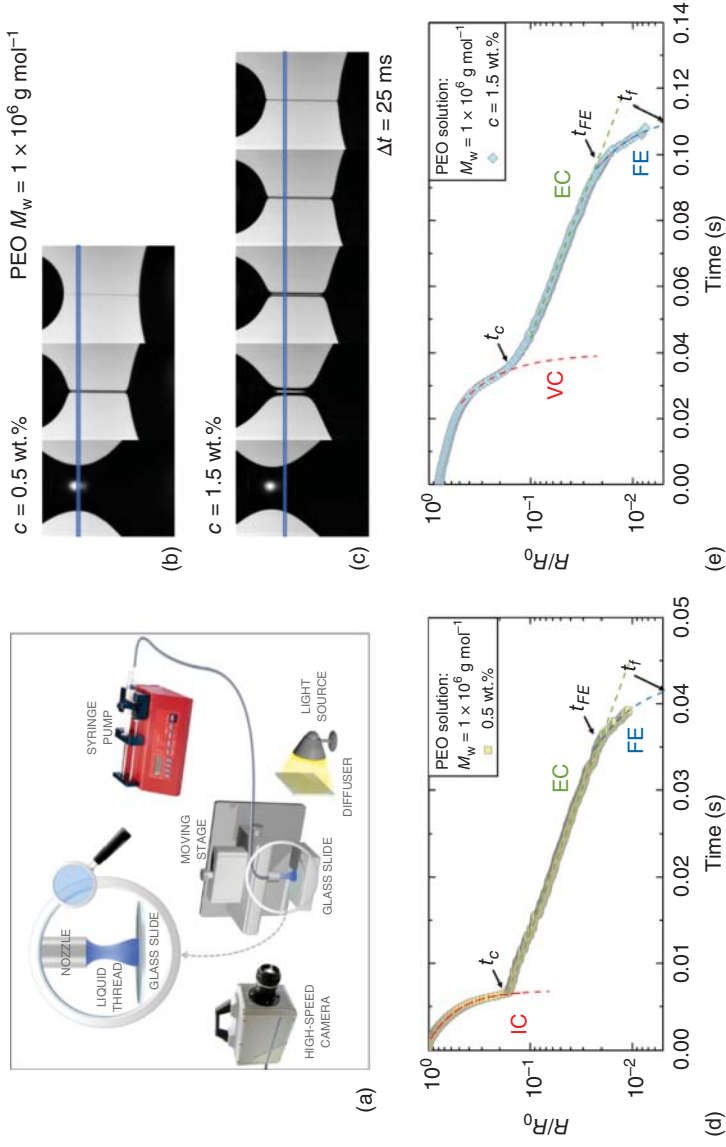
### 3.2 Pinching Dynamics of Unentangled Semi-Dilute PEO Solutions

Figure 4a shows a schematic of the DoS rheometry set-up used for obtaining the neck shape evolution and radius evolution datasets. Figures 4b-e present a comparison between two semi-dilute PEO solutions that show pronounced EC and finite extensibility (FE) or terminal viscoelastocapillary (TVEC), that lead to a substantial delay in pinch-off. As  $Oh < 0.1$  for  $c/c^* < 4$ , the solution with  $c = 0.5$  wt.% regime shows IC regime, whereas the higher concentration  $c = 1.5$  wt.% polymer solution exhibits a VC response [19, 155]. After the initial IC regime, distinct viscoelastic EC and TVEC regimes can be observed and analyzed for  $c = 0.5$  wt.% solution in Figure 4d, even though CaBER measurements are inaccessible for such low viscosity, weak elasticity fluids (see the detailed analysis of the range measurable with CaBER in a contribution by Rodd et al. [25]). The radius evolution data for both solutions (Figure 4d-e) show a clear transition to the EC regime after time  $t_c$ . The transition is delayed for higher concentration PEO solutions with higher viscosity and elasticity. The transition to the EC regime is accompanied by a significant decrease in thinning rate  $\dot{R} = -dR/dt$  and the extension rate defined as  $\dot{\epsilon} = -2\dot{R}(t)/R(t)$ . The radius evolution data in the EC regime appears as a straight line on the semi-log plots.

The form given in the equation for the EC regime includes a timescale,  $t_c$  defined at the onset of the EC regime. Carrying out analysis in this shifted time provides more physically reasonable values for  $G_E$ . We note that  $G_E \neq G \equiv \eta_p \lambda_s$  or the value of  $G_E$  cannot be computed using the product of polymer contribution to solution shear viscosity and shear relaxation time. Furthermore, it follows that the radius at IC/VC to EC transition defines the prefactor in the EC equation in Table 1 (and radius at this first transition  $R_c \approx R_0(G_E R_0 / 2\sigma)^{1/3}$  is also determined by the interplay of elasticity and capillarity). While DoS rheometry allows robust analysis of both EC regime and  $\lambda_E$  values for semi-dilute polymer solutions (as detailed in our previous study [41]), Clasen [177] showed that the corresponding analysis of CaBER data is fraught with larger errors (others showed that comparison with theory often requires the inclusion of a prestretch [103, 120]). Consequently, the timespan between two transitions and the connections with the macromolecular properties and conformational transitions, remain unexplored.

In the EC regime, filament thinning proceeds with a constant extensional rate such that the effective  $Wi_E = \dot{\epsilon} \lambda_E = 2/3$  is the same for all measurements





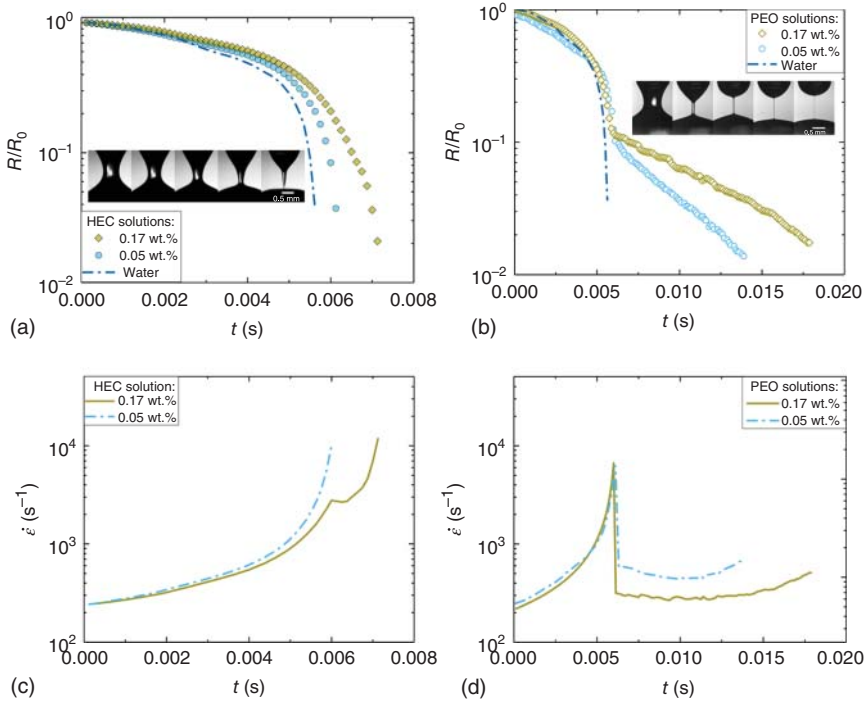
**Figure 4** Dripping-onto-substrate (DoS) rheometry set-up, and representative radius evolution plots and space-time diagrams. (a) DoS rheometry set-up consists of an imaging system that includes a high-speed camera with additional lenses and a dispensing system that consists of a syringe pump connected to a nozzle. (b) The sequence of images for the aqueous PEO solution ( $M_w = 1 \times 10^6 \text{ g mol}^{-1}$  and  $c = 0.5 \text{ wt.}\%$ ) obtained at 8000 fps shows the formation of a slender, cylindrical neck that emerges due to elastocapillary thinning response. (c) The sequence of images for the PEO solution ( $M_w = 1 \times 10^6 \text{ g mol}^{-1}$  and  $c = 1.5 \text{ wt.}\%$ ) shows a delayed break-up in contrast with (b). (d–e) Radius evolution over time plotted for the PEO solutions with  $c = 0.5 \text{ wt.}\%$  and  $c = 1.5 \text{ wt.}\%$ , obtained by analyzing neck shape and neck radius evolution over time. The neck radius is scaled using a nozzle radius,  $2R_0 = 1.27 \text{ mm}$ .

despite molecular weight or concentration variations, even though the thinning rate and the actual extensional rate for each fluid is set by its extensional relaxation time. Though the strain rate exhibits a constant value, the Hencky strain  $\varepsilon = 2 \ln(R_0/R(t))$  increases monotonically, accompanied by a progressive build-up of macromolecular strain and orientation, leading to the emergence of the TVEC regime due to the finite extensibility effects. Though the extensional rate remains constant in the EC regime, it rises after the EC-TVEC transition occurs at the instant  $t_{FE}$ . The TVEC regime yields the value of terminal, steady extensional viscosity and  $Tr^\infty = \eta_E^\infty/\eta$  is the terminal Trouton ratio. The value of Rayleigh time  $t_R$  is  $\sim 2$  ms for PEO solutions (computed using outer nozzle radius), and  $t_f$  refers to the filament lifespan. The existence of steady, terminal extensional viscosity implies an upper bound to the viscoelastic stresses that can be generated from the interplay between the effect of stretching and orientation.

### 3.3 Contrasting Radius Evolution Data for Unentangled HEC and PEO Solutions

Even though the shear viscosity measured for matched dilute concentrations of PEO and HEC are quite similar, neck shape and filament radius evolution characterized using DoS rheometry protocols (see Figure 5a–b) exhibit contrasting behavior. The radius evolution for pure water ( $c/c^* = 0$ , shown as a dash-dotted blue line) exhibits characteristic inertio-capillary (IC) pinching behavior [19, 70, 71, 78, 153, 154]. The two dilute PEO solutions at  $c = 0.05$  wt.% (blue circles, dilute regime,  $c[\eta] = c/c^* \approx 0.3$ ), and  $c = 0.17$  wt.% (gold diamonds at overlap concentration with  $c/c^* \approx 1$ ), respectively, also display an initial IC regime, followed by a distinct transition to an EC regime. The EC regime appears linear in a semi-log plot of filament radius versus time, as shown in Figure 5b. At first glance, the EC response seems to be absent or imperceptible in the radius evolution plots of dilute HEC solutions. However, the neck shape before pinch-off obtained for the dilute HEC solutions is quite distinct from a single sharp cone obtained for water and other low viscosity Newtonian fluids that undergo IC pinching. The image sequence for the HEC solution at the overlap concentration (0.17 wt.%, Figure 5a) reveals that the conical neck is connected to the sessile drop by a slender cylindrical filament in the final stage before the pinch-off event.

A close examination of the neck shapes for an extended range of concentrations for the aqueous HEC solutions shows that the conical neck progressively disappears in favor of slender, cylindrical shape in nondilute solutions of HEC ( $c[\eta] > 1$ ) only after the solution shear viscosity rises to  $\sim 10$  times the solvent viscosity (detailed in a companion paper [189]). In contrast, a slender, cylindrical filament shape arises for the PEO solutions in dilute systems, even at  $c[\eta] = 0.1$ , as described in our earlier papers [40, 41, 77, 79]. However, the presence of a slender, cylindrical filament, a delayed pinch-off (the presence of two distinct regimes for  $c = 0.17$  wt.% solution), and a lack of satellite drop formation show that HEC as an additive alters the pinching dynamics, the extensional rheology response, and the drop size distribution. The contrast in capillarity-driven pinching dynamics and response to extensional flows are further highlighted in the extensional rate versus time plot, as shown in Figures 5c–d. For the 0.05 wt.%



**Figure 5** Contrasting the influence of the three chemistry-dependent macromolecular parameters (flexibility, extensibility, and segmental dissymmetry) on neck shape, radius evolution, and extensional rate variation with time. (a) Radius evolution datasets for two HEC solutions show a slower pinching rate and a delayed pinch-off compared to water. The neck shape, shown for 0.05 wt.% HEC, appears to have a pronounced cone characteristically observed during inertio-capillary pinching. (b) Radius evolution for PEO solutions shows the transition from an inertio-capillary (IC) to elastocapillary (EC) pinching. Although the shear viscosity values of HEC and PEO solutions are nearly matched, the inset shows that slender, cylindrical filament forms in the case of PEO solutions. The filament lifespan,  $t_f = 20$  ms for the aqueous PEO solution, is much longer than  $t_f = 7$  ms for the aqueous HEC solution. Here, the elastocapillary span provides a dominant contribution to the filament lifespan. (c) The extensional rate, determined from the filament radius evolution data, appears to increase monotonically for the HEC solutions, rising to a relatively high value of  $\dot{\epsilon} \approx 10^4 \text{ s}^{-1}$ . Two regimes were observed for the solution with higher concentration ( $c = 0.17$  wt.%). (d) For PEO solutions, the extensional rate exhibits a characteristic increase in the IC pinching regime, and displays a sudden and precipitous drop at the onset of EC behavior. Extensional rate maintains a constant value in the EC regime but rapidly climbs again in the terminal viscoelastocapillary (TVEC) or the finite extensibility regime.

HEC solution, the extensional rate,  $\dot{\epsilon} = -2\dot{R}/R$  computed using the radius evolution data of a pinching filament increases monotonically, whereas the rate data for the 0.17 wt.% HEC solution (at  $c = c^*$ ), appears to show a short-lived EC regime. In contrast, at matched concentrations, the extensional rate increases with time in the IC regime for the PEO solution, but it plunges precipitously after the IC-EC transition, exhibiting a discrete and distinctive shift to a lower rate (Figure 5d).

The contrast in behavior displayed at  $c[\eta] = c/c^* \approx 1$  in Figure 5 is particularly remarkable as any a priori estimates of viscous (matched shear viscosity), elastic (comparable Zimm relaxation time:  $\lambda_Z^{\text{PEO}} = 0.1$  ms and  $\lambda_Z^{\text{HEC}} = 0.07$  ms), and capillary stresses as well as a prediction for pinching dynamics in EC regime would be similar if based on the Entov–Hinch theory or its variants that utilize either shear relaxation time or the same effective relaxation time (for both IC and EC regimes) [19, 44, 88, 89, 95, 103, 166, 175, 225]. Furthermore, the  $\lambda_s$  values cannot be otherwise measured or deduced using shear rheometry in many other cases, including those for the unentangled polymer solutions in relatively low viscosity solvents like water, discussed here. The influence of elasticity for dilute solutions can be gauged based on the estimated value of Zimm relaxation time  $\lambda_z = \frac{1}{\zeta(3\nu)} \frac{[\eta]\eta_s M_w}{RT}$  (for a nondraining, unperturbed coil in a single chain limit). Here the prefactor  $1/\zeta(3\nu) = 1/\sum_{i=1}^{\infty} (1/i^{3\nu})$  depends on the solvent quality exponent,  $\nu$ . However, the estimated Zimm times only give the lowest threshold for the relaxation time as an accurate description of polymer dynamics requires accounting for both concentration-dependent and conformation-dependent hydrodynamic and EV interactions [5–10, 15, 16, 26, 37, 40, 41, 45–47, 77, 79, 190, 191, 215–218, 226–229].

We posit that the discrete transition in the extensional rate versus time data for PEO solutions is a signature of an underlying coil-stretch transition that occurs when the ratio of stretching rate to the relaxation rate (computed using shear relaxation time of unperturbed coils,  $\lambda_s$ ) exceeds the value of  $1/2$  or a critical extensional rate such that  $Wi = \lambda_s \dot{\epsilon}_{c \rightarrow s} > 1/2$ . The measured extensional rate in the EC regime corresponds to a low Weissenberg number  $Wi_s = \lambda_s \dot{\epsilon}_{\text{EC}} < 0.1$  if shear relaxation time is used for the estimate. Prabhakar et al. [26, 45] recently argued that following the coil-stretch transition, the conformation-dependent drag of flexible polymer chains leads to a coil-stretch hysteresis, allowing a lower extensional rate to be effective in preventing the already stretched chains from relaxing back. In other words, the extensional rate in the EC regime stays above the critical extensional rate at the stretch-coil transition, or  $\dot{\epsilon}_{s \rightarrow c} < \dot{\epsilon}_{\text{EC}} < \dot{\epsilon}_{c \rightarrow s}$ . The coil-stretch transition leads to a profound change in the coil conformation, which results in an effectively longer relaxation time of the stretched chains, measured or reported as extensional relaxation time,  $\lambda_E$ . This leads to a high effective Weissenberg number,  $Wi_{\text{EC}} = \lambda_E \dot{\epsilon}_{\text{EC}} \approx 2/3$  in the EC regime. Consequently, the chains continue to experience a sustained stretching in the EC regime, and build-up macromolecular strain, leading to the TVEC (or the finite extensibility) regime that can be analyzed to obtain a steady, terminal extensional viscosity value that is independent of both strain and strain rate. In contrast, for HEC solutions, even though dynamics relatively close to the pinch-off event exhibit a non-Newtonian or viscoelastic response, the discrete jump or overshoot in extensional rate, presumably associated with the changes in macromolecular dynamics after coil-stretch transition, is absent.

Several literature studies recognize that the experimentally obtained radius evolution data for flexible polymer solutions using dripping, jetting or CaBER-like stretched liquid bridge protocols cannot be quantitatively and self-consistently modeled by numerical or analytical solutions based on Oldroyd-B,

FENE-P or Giesekus constitutive models (even if multiple modes are used) [26, 43, 45, 76, 103, 104, 120]. Historically, Entov and Hinch [120] compared their EC expression to the experimental data reported by Liang and Macklay [94]. As the initial VC regime was not resolved in the radius evolution data obtained from stretched liquid bridges [94], fortuitously, the comparison was carried out for  $t_c = 0$  (see EC equation). For nondilute solutions, their assumption  $\lambda_{EC} = \lambda_s$  is somewhat justified. Nevertheless, Entov and Hinch [120] found that including a prestretch,  $P$  in the prefactor (or using a product of  $G$  and  $P$ ) was necessary to match the radius evolution profiles obtained experimentally. Subsequent studies by Anna and McKinley [103], and Tirtaatmajda et al. [43], among others [76, 95] reiterate that the quantitative comparisons are unsuccessful in describing the onset (i.e., the transition point referred here in terms of  $R_c$  and  $t_c$ ), duration (EC span,  $\Delta t_{EC}$ ) and decay constant ( $\lambda_{EC}$ , used to obtain extensional relaxation time,  $\lambda_E = \lambda_{EC}$ ) of the EC regime by use of moduli and relaxation times obtained from shear rheology measurements or theory. A few recent theoretical studies revisit the problem of capillarity-induced pinching by utilizing constitutive models that include finite extensibility but do not show coil-stretch hysteresis [95, 166, 175, 225]; however, comparisons with experiments are not included, the possibility of coil-stretch transition (and hysteresis) is not considered, and the influence of large stretching on relaxation dynamics of stretched polymer dynamics is also not evaluated. The influence of the coil-stretch transition and hysteresis on the concentration-dependent variation of extensional relaxation time, the role of free-surface flows and non-Newtonian fluid mechanics, and the influence of chemical structure are discussed in the later sections.

We contend that in capillarity-driven pinching, the progressive decrease in neck radius leads to a corresponding increase in the applied stress. The changes in extensional rate over time emulate and are influenced by, the corresponding conformational changes in macromolecules. Thus, extensional rheometry protocols based on capillarity-driven pinching can be considered stress-controlled experiments, in contrast to the extensional rate-controlled measurements carried out by Schroeder et al. [8, 9, 16, 215] and by many groups that investigated flow birefringence in stagnation point flows [24, 50, 114, 230]. As the flow fields within pinching filaments emulate the real flows encountered during drop formation and liquid transfer, we suggest that an understanding of coil-stretch transition and hysteresis can be used to outline the quantitative criteria for how the choice of polymer chemistry and molecular weight influence processibility, as seen here for HEC and PEO with comparable molecular weights, and similar coil size or overlap concentration. A significant contrast exists in the value of flexibility of two polymers for the local flexibility as characterized by the Kuhn segment size and the global flexibility characterized by  $N_K$ . A comparison of macromolecular parameters is presented in Table 2 for flexible PEO ( $M_w = 1 \times 10^6$  Da) and the semi-flexible HEC of a comparable molecular weight ( $M_w = 7.2 \times 10^5$  Da).

Likewise, the extensibility,  $L_E^2$  values are nearly two orders of magnitude higher for the PEO solutions. The value of  $L_E^2 = 3840$  is computed for the flexible PEO ( $M_w = 1 \times 10^6$  Da) in contrast with  $L_E^2 = 42$  obtained for the semi-flexible HEC

**Table 2** Macromolecular parameters for aqueous PEO and HEC molecules.

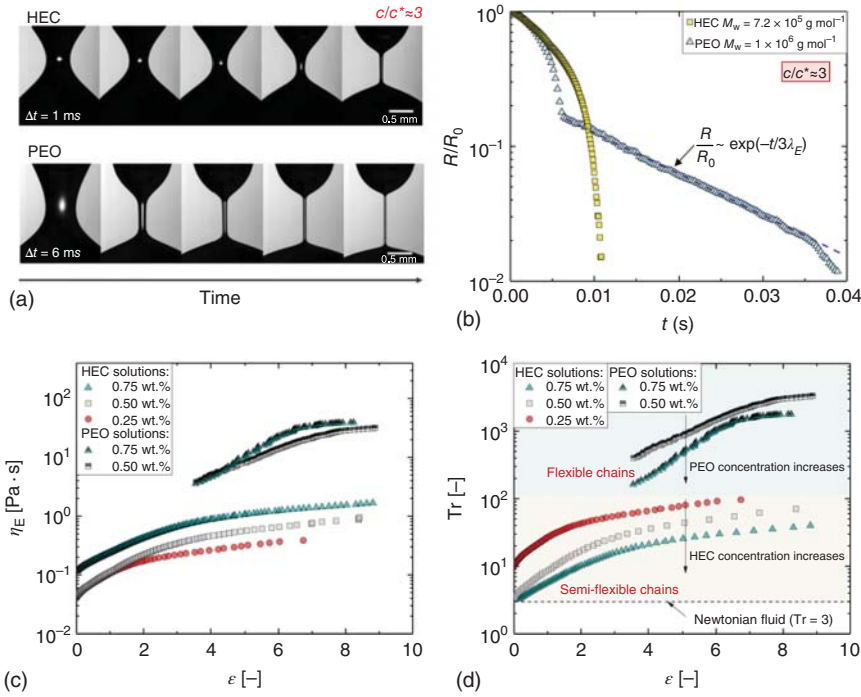
Polymer	PEO	HEC	Reference
$M_w$ (kg mol <sup>-1</sup> ), molecular weight (avg)	1000	720	Average provided by the supplier
$M_0$ (g mol <sup>-1</sup> ), monomer molecular weight	44	272	
$R_g$ (nm), radius of gyration	68	68	224
$\langle R_0^2 \rangle^{1/2}$ (nm), end-to-end distance	167	167	Computed [10]
$b_K$ (nm), Kuhn segment length	1.1	20–60 <sup>a)</sup>	114 231
$d$ (nm), Kuhn segment diameter	0.5	1	Computed [10]
$b_K/d$ , Kuhn segment aspect ratio	2.2	20	Computed [1]
$N_K$ , number of Kuhn segments	9280	70	Computed [124]
$C_\infty$ , characteristic ratio	6.7	21.4	232
$l$ (nm), bond length	1.54	0.77	232
$L_c = R_{max}$ , ( $\mu$ m), contour length	10.2	1.3	Computed [124]
$L_E^2$ , finite extensibility parameter	3720	46	Computed [24]
$\zeta_s/\zeta_c$ , drag coefficient ratio	7.8	1.4	Computed [12]
$[\eta]$ cm <sup>3</sup> g <sup>-1</sup> , intrinsic viscosity	598	598	
$\lambda_z$ (ms), Zimm relaxation time	0.1	0.07	Computed [10]
$\lambda_R$ (ms), Rouse relaxation time	0.14	0.09	Computed [10]

a) 20 is used in this study.

of a comparable molecular weight ( $M_w = 7.2 \times 10^5$  Da). In the present context, for HEC molecules of  $M_w = 720$  kg mol<sup>-1</sup> in water, the ratio of drag coefficients equals 1.4, while for PEO molecules of  $M_w = 1000$  kg mol<sup>-1</sup> in water, the ratio equals 7.8. Thus, the observation of the coil-stretch transition in PEO is expected or predicted based on Eq. (3). Computation using the Eq. (3) suggests that a molecular weight higher than  $10^7$  g mol<sup>-1</sup> is needed to observe the coil-stretch hysteresis in unentangled HEC solutions!

### 3.4 Transient Extensional Viscosity of Aqueous HEC Solutions Measured Using DoS Rheometry

At the matched degree of overlap or  $c/c^*$  value, the radius evolution data for nondilute PEO solutions ( $c > c^*$ ) also exhibit a pronounced EC regime in contrast to the HEC solutions as shown in Figure 6. For the PEO solutions, EC span,  $\Delta t_{EC}$  makes the primary contribution to filament lifespan,  $t_f$ . In contrast, for HEC solutions,  $\Delta t_{EC} \ll t_f$ , and the short  $\Delta t_{EC}$  results in a relatively short filament lifespan for dilute solutions as well as for the data shown in Figure 6a for semi-dilute solutions at  $c/c^* = 3$  (even though the shear viscosity of the HEC solution is marginally higher). Apparent extensional viscosity of HEC solutions was determined and compared with the extensional viscosity calculated for PEO solutions, as shown in Figure 6. As the interplay of tensile viscoelastic stresses  $\eta_E \dot{\epsilon}$



**Figure 6** Comparison of the neck shape, radius evolution, extensional viscosity, and Trouton ratio as a function of Hencky strain plots for semi-dilute aqueous PEO and HEC solutions. (a) Image sequence contrasts the neck shape and shape evolution at  $c/c^* = 3$ . The time elapsed between progressive snapshots is  $\Delta t = 1$  ms for the HEC solution and  $\Delta t = 6$  ms for the PEO solution. (b) Radius evolution in time data show striking contrast and the dashed line represents the elastocapillary fit to the PEO data using expression included in Table 1. The PEO solution thins remarkably slowly, even though the shear viscosity of the HEC solution is higher at  $c/c^* = 3$ . (c) Lower extensional viscosity values are measured for the solutions of less flexible HEC than PEO at matched concentrations (and matched Berry number). (d) The Trouton ratio computed using the ratio of extensional viscosity shown in (c) and zero shear viscosity values show that the comparative strain-hardening and overall extensional viscosity of the aqueous solutions of flexible polymers are much higher than those obtained for HEC solutions. For these nondilute solutions, the Trouton ratio decreases as polymer concentration increases.

and the capillary stress  $\sigma/R(t)$  determines the radius evolution for viscoelastic solutions, a transient extensional viscosity measure,  $\eta_E = \eta_E^+(t, \dot{\epsilon})$  (also referred to as tensile growth coefficient) can be obtained by using the following equation:

$$\eta_E = \frac{\sigma}{R(t)\dot{\epsilon}(t)} = \frac{\sigma}{-2\dot{R}(t)} \quad (6)$$

Although the extensional rate stays constant during the EC regime, the Hencky strain or the total accumulated strain in the liquid filament,  $\epsilon = 2 \ln(R_0/R(t))$  increases steadily, and hence conventionally [19], the measured apparent extensional viscosity in capillary-thinning studies is plotted as a function of Hencky strain, as shown in Figure 6c for HEC and PEO solutions. Both flexible PEO and the semi-flexible HEC solutions exhibit considerable

extensional strain-hardening response, even though the shear viscosity exhibits rate-dependent decrease associated with shear thinning caused by orientation of mildly perturbed coils. Furthermore, the plotted data show that at a comparable degree of overlap (i.e., the same Berry number), the HEC solutions exhibit lower extensional viscosity values than PEO solutions. As the concentration of HEC increases, an increase in both transient and terminal extensional viscosity is observed.

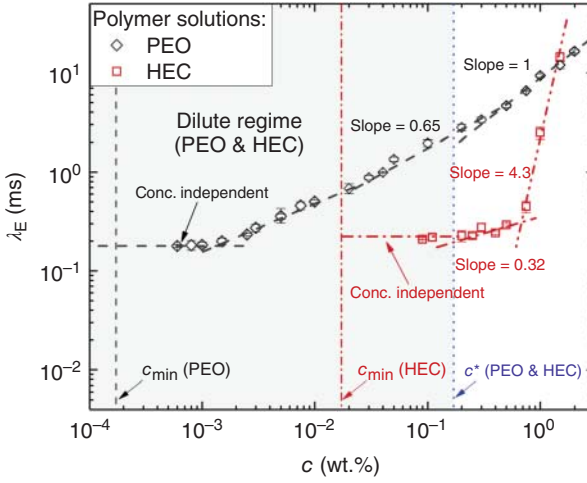
For the range of concentrations shown in Figure 6c, the shear viscosity data show a relatively mild shear-thinning. Therefore, zero shear viscosity  $\eta_0$  can be used to plot a dimensionless extensional viscosity measure, known as the Trouton ratio,  $\text{Tr} = \eta_E(\dot{\epsilon}, \epsilon, t)/\eta_0$  (plotted in Figure 6d). For these nondilute solutions, the value of the Trouton ratio decreases as concentration increases. Additionally, the Trouton ratios obtained for semi-dilute solutions of a less flexible polymer (HEC) are several orders of magnitude lower despite having a higher zero shear viscosity than PEO solutions of the same concentrations. Thus, the viscoelastic stresses contributed by extended HEC polymers are much lower than those contributed by stretched PEO chains. The Trouton ratio values for PEO solutions ( $100 < \text{Tr} < 5000$ ) are much higher than for HEC ( $\text{Tr} \leq 100$ ), as shown in Figure 6.

### 3.5 Concentration-Dependent Extensional Relaxation Times

EC fits to the radius evolution data yield the concentration-dependent values of extensional relaxation times for both polymers, plotted in Figure 7. The absolute value of the extensional relaxation time measured for aqueous PEO solutions at a matched concentration by weight and matched Berry number is much higher. The extensional relaxation time for aqueous PEO solutions shows the two scaling exponents characteristic of dilute ( $\lambda_E \propto c^{0.65}$ ; for  $0.1c^* < c < c^*$ ) and intrinsically semi-dilute, entangled PEO solutions ( $\lambda_E \propto c$  for  $c > c^*$ ) previously described and determined [40, 41] using DoS rheometry studies. We argued that the scaling laws arise from partial screening of EV interactions in the dilute regime, whereas for  $c > c^*$  the EV interactions get effectively screened at all length scales [41]. In dilute solutions,  $\lambda_E \propto c^{0.65}$  was also reported by Tirtaatmadja et al. [43] using dripping experiments for PEO in the glycerol–water mixture and by Clasen et al. [44] for dilute polystyrene solutions in diethyl phthalate (both studies used good solvents more viscous than water). However, as the HEC chains do not undergo coil-stretch transition, a weaker concentration dependence  $\lambda_E \propto c^{0.32}$  associated with the Rouse–Zimm chain in a good solvent (blob model) is observed in the semi-dilute regime ( $c^* < c < c_e$ ) [1]. The extensional relaxation time values for the entangled HEC solutions ( $c > c_e$ ) exhibit a substantial increase with concentration  $\lambda_E \propto c^{4.3}$  that mimics the exponent observed for a concentration-dependent increase in specific viscosity  $\lambda_E \propto \eta_{\text{sp}} \propto c^{4.3}$ . Furthermore, both coil–coil overlap and EV interactions are influenced by the degree of stretching, conformational anisotropy, and tension applied to the chains, and standard blob theory was not designed to account for all three effects.

A comparison of HEC and PEO solutions shows that the concentration-independent values of  $\lambda_E$  can be measured at much lower concentrations





**Figure 7** Concentration-dependent variations in relaxation time values for aqueous HEC and PEO solutions. Extensional relaxation times for the aqueous HEC solutions are found to be lower than the values for the aqueous PEO solutions at matched concentration and matched Berry numbers. However, as the HEC solutions can entangle at a much lower concentration, the relaxation time shows a stronger concentration-dependent variation above  $c > 0.5$  wt.%. The PEO solutions show three regimes: (i) concentration-independent regime below  $c = 0.001$  wt.%, (ii) an extended regime with concentration-dependent increase captured by exponent 0.65 for  $0.1c^* < c < c^*$ , and (iii) intrinsically semi-dilute solution behavior above  $c^*$ . The plot identifies a theoretical estimate for critical minimum concentration,  $c_{\min}$  needed for generating elastic stress that leads to the appearance of the elastocapillary regime. The existence of a concentration-independent regime is also noted.

for PEO than are possible for HEC. Notwithstanding any imaging and image analysis challenges, Clasen et al. [44] determined that there exists a critical concentration  $c_{\min} = (3M_w\eta_s)/(2RT\lambda_zL_E^2)$  below which the polymer carries less stress than a viscous solvent (even when the chains become fully stretched) and the extensional relaxation time can no longer be deduced. We can recast the formula for  $c_{\min}$  using the formula for Zimm relaxation time as  $c_{\min}/c^* \approx 3/L_E^2$ . Using Table 2, we estimate,  $c_{\min} = 1.4 \times 10^{-4}$  wt.% for PEO solutions, and nearly two orders of magnitude higher concentration  $c_{\min} = 1.4 \times 10^{-2}$  wt.% for HEC solutions. Thus, the calculated  $c_{\min}$  concentration for HEC or PEO is only 6.4 times lower than the minimum concentration plotted in Figure 7.

### 3.6 Segmental Dissymmetry and Stretched Overlap Concentration

The experimentally determined value of HEC concentration at which the topological entanglements begin to exist in the polymer solution was found to be  $c \approx 0.5$  wt.% or at  $c_e/c^* \approx 3$ . It is well-known that semi-dilute solutions have large concentration fluctuations, and above a critical  $c^{**}$ , the polymer solution behavior can be described using a mean-field theory for concentrated solutions. Since the value of  $c^{**}/c^* \approx N_K^{3\nu-1}(d^2/b_K^2)^{3\nu-1}$  depends on the Kuhn segment shape and size (assuming EV value for a thermal limit,  $b_K^2d$  to get an upper limit),

we can rewrite the expression in terms of segmental dissymmetry as follows,  $c^{**}/c^* \approx (N_K/S_d)^{3\nu-1}$ . The lower absolute values of  $c^{**}$  (and possibly entanglement concentration) result from fewer Kuhn segments and larger segmental dissymmetry for polysaccharides. More recently, Dorfman and coworkers [204] determined how the effective EV parameter (or the solvent quality exponent) itself depends on the number of Kuhn segments and the ratio of Kuhn segment length to diameter: thus, effectively on  $S_d$ .

The extensional relaxation time data for both HEC and PEO solutions exhibit a nearly constant value below a material-dependent concentration value we christen as *stretched overlap concentration*,  $c_s^*$  highlighting that for stretched chains, the inter-chain contacts are present even if the solution is considered nominally dilute based on the  $c^*$  value computed using the unperturbed coil size. We postulate that the stretched overlap concentration,  $c_s^*$  can be estimated using theory for semi-dilute solutions for rod-like polymers. According to Doi and Edwards [2], the semi-dilute regime for rod-like polymers spans a range between (i) the concentration at which the average distance between polymers  $\vartheta^{-1/3}$  is less than the rod length or  $\vartheta_1 R_s^3 < 1$ , and (ii) the concentration  $\vartheta_2 d R_s^2 < 1$  such that the constraint on their crossing each other influences the dynamic properties of finite-diameter rods. The experimental results and theoretical arguments suggest that the EC regime arises long before the coils get fully stretched. We utilize the second expression to obtain an overlap concentration for stretched chains as  $c_s^*/c^* \approx 4R_g^3/dR_s^2$  or  $c_s^*/c^* \approx N_K^v S_d^{1/2}/L_E^2 = N_K S_d^{1/2}/L_E^3$ . The estimated value of  $c_s^*/c^* \approx 0.006$  for PEO solutions is within a factor of 2 of the experimentally observed value. Likewise, Figure 7 data shows that the estimated value  $c_s^*/c^* \approx 0.3$  for the HEC solutions is quite close to the experimentally observed value of both stretched and standard overlap concentrations.

## 4 Conclusions

A comparison of shear and extensional rheology responses of the aqueous solutions of a semi-flexible polysaccharide, 2-hydroxyethylcellulose (HEC) against the aqueous solutions of flexible poly(ethylene oxide) (PEO) is carried out such that the equilibrium coil size and overlap concentration (or intrinsic viscosity) are nearly matched. Hence, a matched concentration by weight corresponds to a matched value of the Berry number. As expected, the steady shear viscosity of both polymers is comparable at matched concentrations in the dilute regime. Steady shear viscosity of nondilute HEC solutions was higher than the viscosity of PEO solutions as HEC solutions cross over into the entangled regime at a lower concentration than PEO solutions. Aqueous solutions of both polymers show a concentration-dependent increase in extensional relaxation time and filament lifespan (or pinch-off time). Even though the shear viscosity values are matched for the dilute solutions, the PEO solutions exhibit a longer filament lifespan, and higher values of both extensional relaxation time and extensional viscosity. At all concentrations, the PEO solutions exhibit higher

values of the terminal extensional viscosity, even though the shear viscosity of nondilute HEC solutions ( $c > c^*$ ) is much higher than the PEO solutions at matched concentrations (and  $c/c^*$  values). The nondilute HEC solutions exhibit a pronounced shear-thinning behavior. For industrially relevant concentrations (typical  $c < 1$  wt.%), the HEC solutions also exhibit a shorter filament lifespan than the PEO solutions. Both attributes make HEC advantageous as a rheology modifier for dispensing applications: at low deformations, the dispersion behaves like a high viscosity fluid and does not “run” or spread (helps in controlling sagging in paints), whereas, at higher rates encountered during pumping or dispensing, the dispersion flows relatively easily. Furthermore, significantly faster pinching rate and shorter filament lifespan of the unentangled HEC solutions than the unentangled PEO solutions (compared here at matched concentration for matched unperturbed coil size) make HEC and other polysaccharides preferred candidates as rheology modifiers for spraying, printing, and painting applications.

Aqueous PEO solutions display a very pronounced transition from inertio-capillary to a long EC regime in radius evolution of pinching filament for dilute and some semi-dilute solutions (for dimensionless concentration values up to  $c/c^* = 5$ ). We argue that the transition is associated with a discrete change in extensional rate to a lower value, associated with the changes in macromolecular dynamics after undergoing coil-stretch transition. In contrast, the radius evolution data of pinching filament of the aqueous solutions of semi-flexible HEC display only a weak, relatively short-lived EC tail, and the extensional rate displays a nearly monotonic increase with time as the pinch-off event is approached, implying the absence of coil-stretch transition in this case. The calculation of coil-stretch transition and hysteresis criteria using the ratio of drag coefficients requires the value of an additional length scale,  $d$  that represents the hydrodynamic diameter of a Kuhn segment. Though value of  $d$  is often unknown, we propose to use the knowledge of packing length,  $p$  that is an additional, but known length scale required for describing entangled solution and melt rheology. We rewrite the ratio of Kuhn segment length to diameter in terms of an effectively comparable ratio of ratio of Kuhn length to packing length that we christened as segmental dissymmetry,  $S_d$ . Even if the coil-size, dilute solution rheology or values of Zimm relaxation time are matched, the coil-stretch transitions are most likely to occur for the more flexible polymers that have smaller segmental dissymmetry.

We postulate and argue that the same set of three macromolecular parameters – flexibility, extensibility, and segmental dissymmetry – enable us to distill the influence of chemical structure on macromolecular dynamics and viscoelastic effects associated with coil-stretch transition and hysteresis [8, 9, 16, 215, 217], as well as entanglements [30, 193, 219] and consequently, on the shear and extensional rheological response, capillarity-driven pinching dynamics, and processability. We posit that the constitutive models that explicitly include conformation-dependent drag, finite extensibility, and the physics of coil-stretch transition (and hysteresis) could prove beneficial for capturing the nonmonotonic behavior of extensional rate displayed by the PEO solutions in response to a progressively increasing capillarity-induced stress. However, for

the unentangled HEC solutions, the shear relaxation time values estimated using the theory of polymer dynamics as well as using fits to the steady shear viscosity data are comparable to the values of  $\lambda_E$  extracted from the relatively short-lived EC regime. We surmise that the capillarity-driven pinching for HEC solutions is more amenable to analysis by constitutive models based on a single relaxation time ( $\lambda_E = \lambda_s$ ) as long as the finite extensibility effects are included to capture the underlying macromolecular physics. We anticipate that our data and analysis will help in further development of new constitutive models and deeper understanding of how chemical structure and solvent-polymer interactions, as imbibed into three macromolecular properties (flexibility, extensibility, and segmental dissymmetry) affect the static and dynamic properties of polymers in solution.

## Acknowledgments

CM and VS would like to acknowledge funding support by the PPG and the 3M nontenured faculty award. JD was supported by the start-up funds and Teaching Assistantship by the Departments of Chemical Engineering and Chemistry at UIC. JD is currently affiliated with Argonne National Laboratory and Pritzker School of Molecular Engineering at the University of Chicago as a postdoctoral researcher supervised by Prof. Matt Tirrell.

## References

- 1 Rubinstein, M. and Colby, R.H. (2003). *Polym. Physics*. New York: Oxford University Press.
- 2 Doi, M. and Edwards, S.F. (1986). *The Theory of Polymer Dynamics*, 406. New York: Oxford University Press.
- 3 de Gennes, P.-G. (1979). *Scaling Concepts in Polymer Physics*. Ithaca: Cornell University Press.
- 4 Lodge, T.P. and Muthukumar, M. (1996). *J. Phys. Chem.* 100 (31): 13275–13292.
- 5 Muthukumar, M. (2017). *Macromolecules* 50 (24): 9828–9560.
- 6 Wang, Z.-G. (2017). *Macromolecules* 50 (23): 9073–9114.
- 7 Prakash, J.R. (2019). *Curr. Opin. Colloid Interface Sci.* 43: 63–79.
- 8 Schroeder, C.M. (2018). *J. Rheol.* 62 (1): 371–403.
- 9 Shaqfeh, E.S.G. (2005). *J. Non-Newtonian Fluid Mech.* 130 (1): 1–28.
- 10 Larson, R.G. (2005). *J. Rheol.* 49 (1): 1–70. doi: 10.1122/1.1835336.
- 11 Rasmussen, H.K., Wingstrand, S.L., and Hassager, O. (2019). *Rheol. Acta* 58 (6): 333–340.
- 12 Nguyen, T.Q. and Kausch, H.H. (1999). *Flexible Polymer Chains in Elongational Flow: Theory and Experiment*. Berlin: Springer-Verlag.
- 13 Petrie, C.J.S. (2006). *J. Non-Newtonian Fluid Mech.* 137 (1–3): 1–14. doi: 10.1016/j.jnnfm.2006.01.010.
- 14 Petrie, C.J.S. (1979). *Elongational Flows*. London: Pitman.

- 15 de Gennes, P.G. (1974). *J. Chem. Phys.* 60 (12): 5030–5042.
- 16 Schroeder, C.M., Babcock, H.P., Shaqfeh, E.S.G., and Chu, S. (2003). *Science* 301 (5639): 1515–1519.
- 17 Owens, M.S., Vinjamur, M., Scriven, L.E., and Macosko, C.W. (2011). *J. Non-Newtonian Fluid Mech.* 166 (19–20): 1123–1128.
- 18 Kumar, S. (2014). *Ann. Rev. Fluid. Mech.* 47 (1): 67–94.
- 19 McKinley, G.H. (2005). *Rheol. Rev.* 1–48.
- 20 Graham, M.D. (2003). *Phys. Fluids* 15: 1702.
- 21 Matsumiya, Y. and Watanabe, H. (2020). *Prog. Polym. Sci.* 112: 101325.
- 22 Sridhar, T. (1990). *J. Non-Newtonian Fluid Mech.* 35 (2): 85–92.
- 23 James, D.F. and Walters, K. (1994). In: *Techniques of Rheological Measurement* (ed. A.A. Collyer), 33–53. New York: Elsevier.
- 24 Sharma, V., Haward, S.J., Serdy, J. et al. (2015). *Soft Matter* 11 (16): 3251–3270.
- 25 Rodd, L.E., Scott, T.P., Cooper-White, J.J., and McKinley, G.H. (2005). *Appl. Rheol.* 15 (1): 12–27.
- 26 Prabhakar, R., Gadkari, S., Gopesh, T., and Shaw, M.J. (2016). *J. Rheol.* 60 (3): 345–366.
- 27 Watanabe, H. (1999). *Prog. Polym. Sci.* 24 (9): 1253–1403.
- 28 Schieber, J.D. and Andreev, M. (2014). *Annu. Rev. Chem. Biomol. Eng.* 5: 367–381.
- 29 Larson, R.G. (1988). *Constitutive Equations for Polymer Solutions and Melts*. Boston: Butterworth Publishers.
- 30 Fetters, L.J., Lohse, D.J., Richter, D. et al. (1994). *Macromolecules* 27 (17): 4639–4647.
- 31 Desai, P.S. and Larson, R.G. (2014). *J. Rheol.* 58 (1): 255–279.
- 32 Wingstrand, S.L., Alvarez, N.J., Huang, Q., and Hassager, O. (2015). *Phys. Rev. Lett.* 115 (7): 078302.
- 33 Nielsen, J.K., Rasmussen, H.K., Hassager, O., and McKinley, G.H. (2006). *J. Rheol.* 50 (4): 453–476.
- 34 Bhattacharjee, P.K., Nguyen, D.A., McKinley, G.H., and Sridhar, T. (2003). *J. Rheol.* 47 (1): 269–290.
- 35 Bhattacharjee, P.K., Oberhauser, J.P., McKinley, G.H. et al. (2002). *Macromolecules* 35 (27): 10131–10148.
- 36 Dinic, J. and Sharma, V. (2020). *Macromolecules* 53: 3424–3437.
- 37 Jimenez, L.N., Dinic, J., Parsi, N., and Sharma, V. (2018). *Macromolecules* 51 (14): 5191–5208.
- 38 Jimenez, L.N., Martínez Narváez, C.D.V., and Sharma, V. (2020). *Phys. Fluids* 32: 012113.
- 39 Martínez Narváez, C.D.V., Dinic, J., Lu, X. et al. (2021). *Macromolecules* 54: 6372–6388.
- 40 Dinic, J., Zhang, Y., Jimenez, L.N., and Sharma, V. (2015). *ACS Macro Lett.* 4 (7): 804–808.
- 41 Dinic, J., Biagioli, M., and Sharma, V. (2017). *J. Polym. Sci. Part B Polym. Phys.* 55 (22): 1692–1704.
- 42 Dinic, J. and Sharma, V. (2020). *Macromolecules* 53: 4821–4835.

- 43 Tirtaatmadja, V., McKinley, G.H., and Cooper-White, J.J. (2006). *Phys. Fluids* 18 (4): 043101.
- 44 Clasen, C., Plog, J.P., Kulicke, W.M. et al. (2006). *J. Rheol.* 50 (6): 849–881.
- 45 Prabhakar, R., Sasmal, C., Nguyen, D.A. et al. (2017). *Phys. Rev. Fluids* 2 (1): 011301.
- 46 Somani, S., Shaqfeh, E.S.G., and Prakash, J.R. (2010). *Macromolecules* 43 (24): 10679–10691. doi: 10.1021/ma1019945.
- 47 Ryskin, G. (1987). *J. Fluid Mech.* 178: 423–440.
- 48 Yarín, A.L. (1993). *Free Liquid Jets and Films: Hydrodynamics and Rheology*. Longman Scientific & Technical.
- 49 Odell, J.A. and Carrington, S.P. (2006). *J. Non-Newtonian Fluid Mech.* 137: 110–120.
- 50 Keller, A. and Odell, J.A. (1985). *Colloid. Polym. Sci.* 263 (3): 181–201.
- 51 Garrepally, S., Jouenne, S., Olmsted, P.D., and Lequeux, F. (2020). *J. Rheol.* 64 (3): 601–614.
- 52 Vadillo, D.C., Mathues, W., and Clasen, C. (2012). *Rheol. Acta* 51 (8): 755–769.
- 53 Yaoita, T., Isaki, T., Masubuchi, Y. et al. (2012). *Macromolecules* 45 (6): 2773–2782.
- 54 Dumitriu, S. (2005). *Polysaccharides: Structural Diversity and Functional Versality*, 2e. New York: Marcel Dekker.
- 55 Lapasin, R. and Pricl, S. (1995). *Rheology of Industrial Polysaccharides: Theory and Applications*. London: Chapman & Hall.
- 56 Clasen, C. and Kulicke, W.M. (2001). *Prog. Polym. Sci.* 26 (9): 1839–1919.
- 57 Kaneda, I. (2017). *Rheology of Biological Soft Matter*. Tokyo: Springer.
- 58 Braun, D.D. and Rosen, M.R. (2013). *Rheology Modifiers Handbook: Practical Use and Application*. Elsevier.
- 59 Kamide, K. (2005). *Cellulose and Cellulose Derivatives: Molecular Characterization and its Applications*. Amsterdam: Elsevier.
- 60 Macosko, C.W. (1994). *Rheology: Principles, Measurements and Applications*. New York: VCH Publishers Inc.
- 61 Jimenez, L.N., Narváez, C.D.M., Xu, C. et al. (2021). *Soft Matter* 17 (20): 5197–5213.
- 62 Jimenez, L.N., Narváez, C.D.V.M., Xu, C. et al. (2021). *Surface Science and Adhesion in Cosmetics* (ed. K. Mittal and H. Bui). Scrivener Publishing/Wiley
- 63 Eley, R.R. (2005). *Rheol. Rev.* 173–240.
- 64 Eley, R.R. (2019). *J. Coat. Technol. Res.* 16 (2): 263–305.
- 65 Lambourne, R. and Striven, T.A. (1999). *Paint and Surface Coatings: Theory and Practice*, 2e. Cambridge, UK: Woodhead Publishing Ltd.
- 66 Trouton, F.T. (1906). *Proc. R. Soc. Lond. A* 77: 426–440.
- 67 Fano, G. (1908). *Arch. Fisiol.* 5: 365–370.
- 68 Green, H. (1941). *Ind. Eng. Chem. Anal. Ed.* 13 (9): 632–639.
- 69 Bhat, P.P., Appathurai, S., Harris, M.T. et al. (2010). *Nat. Phys.* 6 (8): 625–631.
- 70 Eggers, J. (1997). *Rev. Mod. Phys.* 69 (3): 865–929.

- 71 Eggers, J. and Fontelos, M.A. (2015). *Singularities: Formation, Structure, and Propagation*, vol. 53. Cambridge, UK: Cambridge University Press.
- 72 Basaran, O.A., Gao, H., and Bhat, P.P. (2013). *Ann. Rev. Fluid Mech.* 45: 85–113.
- 73 Basaran, O.A. (2002). *AIChE J.* 48 (9): 1842–1848.
- 74 Duxenneuner, M.R., Fischer, P., Windhab, E.J., and Cooper-White, J.J. (2008). *Biomacromolecules* 9 (11): 2989–2996.
- 75 Keshavarz, B., Sharma, V., Houze, E.C. et al. (2015). *J. Non-Newtonian Fluid Mech.* 222: 171–189.
- 76 Sharma, V., Ardekani, A. M., and McKinley, G. H. (2010). Beads on a string structures and extensional rheometry using jet break-up. *5th Pacific Rim Conference on Rheology (PRCR-5)*, Sapporo, Japan, 2010.
- 77 Dinic, J., Jimenez, L.N., and Sharma, V. (2017). *Lab Chip* 17: 460–473.
- 78 Dinic, J. and Sharma, V. (2019). *Phys. Fluids* 31 (2): 021211.
- 79 Dinic, J. and Sharma, V. (2019). *Proc. Natl. Acad. Sci. U.S.A.* 116 (18): 8766–8774.
- 80 Clasen, C., Eggers, J., Fontelos, M.A. et al. (2006). *J. Fluid Mech.* 556: 283–308.
- 81 Clasen, C., Phillips, P.M., and Palangetic, L. (2012). *AIChE J.* 58 (10): 3242–3255.
- 82 Torres, M.D., Hallmark, B., Wilson, D.I., and Hilliou, L. (2014). *AIChE J.* 60 (11): 3902–3915. doi: 10.1002/aic.14611.
- 83 Gilbert, L., Loisel, V., Savary, G. et al. (2013). *Carbohydr. Polym.* 93 (2): 644–650.
- 84 Savary, G., Grisel, M., and Picard, C. (2016). In: *Natural Polymers: Industry Techniques and Applications* (ed. O. Olatunji), 219–261. Springer.
- 85 Morozova, S., Schmidt, P.W., Metaxas, A. et al. (2018). *ACS MacroLett.* 7 (3): 347–352.
- 86 Torres, M.D., Hallmark, B., and Wilson, D.I. (2014). *Food Hydrocoll.* 40: 85–95.
- 87 Bazilevsky, A. V., Entov, V. M., and Rozhkov, A. N. (1990). Liquid filament microrheometer and some of its applications. *Third European Rheology Conference and Golden Jubilee Meeting of the British Society of Rheology*, Edinburgh, UK, 1990; Elsevier: Edinburgh, UK, 1990; 41–43.
- 88 Stelter, M., Brenn, G., Yarin, A.L. et al. (2000). *J. Rheol.* 44 (3): 595–616.
- 89 Stelter, M., Brenn, G., Yarin, A.L. et al. (2002). *J. Rheol.* 46 (2): 507–527.
- 90 Bazilevskii, A.V., Entov, V.M., and Rozhkov, A.N. (2001). *Polym. Sci. A* 43 (7): 716–726.
- 91 Bazilevsky, A.V., Entov, V.M., and Rozhkov, A.N. (2011). *Fluid Dyn.* 46 (4): 613–622.
- 92 Schummer, P. and Tebel, K.H. (1982). *Rheol. Acta* 21 (4–5): 514–516.
- 93 Schummer, P. and Tebel, K.H. (1983). *J. Non-Newtonian Fluid Mech.* 12 (3): 331–347.
- 94 Liang, R.F. and Mackley, M.R. (1994). *J. Non-Newtonian Fluid Mech.* 52 (3): 387–405.
- 95 Ardekani, A., Sharma, V., and McKinley, G.H. (2010). *J. Fluid Mech.* 665: 46–56.

- 96 Miller, E., Clasen, C., and Rothstein, J.P. (2009). *Rheol. Acta* 48 (6): 625–639.
- 97 Rothstein, J.P. (2008). *Rheol. Rev.* 1–46.
- 98 Rothstein, J.P. (2003). *J. Rheol.* 47 (5): 1227–1247.
- 99 Kim, N.J., Pipe, C.J., Ahn, K.H. et al. (2010). *Korea-Australia Rheol. J.* 22 (1): 31–41.
- 100 Chellamuthu, M., Arndt, E.M., and Rothstein, J.P. (2009). *Soft Matter* 5 (10): 2117–2124.
- 101 Ma, A.W.K., Chinesta, F., Tuladhar, T., and Mackley, M.R. (2008). *Rheol. Acta* 47 (4): 447–457. doi: 10.1007/s00397-007-0247-y.
- 102 Tsentlovich, D.E., Ma, A.W.K., Lee, J.A. et al. (2016). *Macromolecules* 49 (2): 681–689.
- 103 Anna, S.L. and McKinley, G.H. (2001). *J. Rheol.* 45 (1): 115–138.
- 104 Amarouchene, Y., Bonn, D., Meunier, J., and Kellay, H. (2001). *Phys. Rev. Lett.* 86 (16): 3558–3561.
- 105 Galindo-Rosales, F.J., Alves, M.A., and Oliveira, M.S.N. (2013). *Microfluid. Nanofluid.* 14 (1–2): 1–19.
- 106 Vadillo, D.C., Tuladhar, T.R., Mulji, A.C. et al. (2010). *J. Rheol.* 54: 261–282.
- 107 Greiciunas, E., Wong, J., Gorbatenko, I. et al. (2017). *J. Rheol.* 61 (3): 467–476.
- 108 Fernando, R.H., Xing, L.L., and Glass, J.E. (2001). *Prog. Org. Coat.* 42 (3–4): 283–288.
- 109 Christanti, Y. and Walker, L.M. (2006). *At. Sprays* 16 (7): 777–790.
- 110 Ashgriz, N. (2011). *Handbook of Atomization and Sprays: Theory and Applications*. New York: Springer.
- 111 Keshavarz, B., Houze, E.C., Moore, J.R. et al. (2016). *Phys. Rev. Lett.* 117 (15): 154502.
- 112 Palangetic, L., Reddy, N.K., Srinivasan, S. et al. (2014). *Polymer* 55 (19): 4920–4931.
- 113 Fang, Y., Dulaney, A.D., Gadley, J. et al. (2015). *Polymer* 73: 42–51.
- 114 Haward, S.J., Sharma, V., Butts, C.P. et al. (2012). *Biomacromolecules* 13 (5): 1688–1699.
- 115 Christanti, Y. and Walker, L.M. (2001). *J. Non-Newtonian Fluid Mech.* 100 (1–3): 9–26.
- 116 Christanti, Y. and Walker, L.M. (2002). *J. Rheol.* 46 (3): 733–748. doi: 10.1122/1.1463418.
- 117 Bousfield, D.W., Keunings, R., Marrucci, G., and Denn, M.M. (1986). *J. Non-Newtonian Fluid Mech.* 21 (1): 79–97.
- 118 McKinley, G.H. and Sridhar, T. (2002). *Annu. Rev. Fluid Mech.* 34: 375–415.
- 119 Martínez Narváez, C.D.V., Mazur, T., and Sharma, V. (2021). *Soft Matter* 17: 6116–6126.
- 120 Entov, V.M. and Hinch, E.J. (1997). *J. Non-Newtonian Fluid Mech.* 72: 31–54.
- 121 Wüstenberg, T. (2014). *Cellulose and Cellulose Derivatives in the Food Industry: Fundamentals and Applications*. John Wiley & Sons.
- 122 Glass, J.E. (1986). *Water Soluble Polymers: Beauty with Performance*. Washington, DC: American Chemical Society.



- 123 Williams, P.A. (2007). *Handbook of Industrial and Water Soluble Polymers*. Oxford: Blackwell Publishing Ltd.
- 124 Larson, R.G. (1999). *The Structure and Rheology of Complex Fluids*. New York: Oxford University Press.
- 125 Barnes, H.A., Hutton, J.F., and Walters, K. (1989). *An Introduction to Rheology*. Amsterdam: Elsevier Science Publishers B. V.
- 126 Ferry, J.D. (1980). *Viscoelastic Properties of Polymers*, 3e. New York: Wiley.
- 127 Shaqfeh, E.S.G. (1996). *Annu. Rev. Fluid Mech.* 28 (1): 129–185.
- 128 Larson, R.G., Shaqfeh, E.S.G., and Muller, S.J. (1990). *J. Fluid Mech.* 218: 573–600.
- 129 Muller, S.J., Larson, R.G., and Shaqfeh, E.S.G. (1989). *Rheol. Acta* 28 (6): 499–503.
- 130 Larson, R.G. (1992). *Rheol. Acta* 31 (3): 213–263.
- 131 McKinley, G.H., Pakdel, P., and Öztekin, A. (1996). *J. Non-Newtonian Fluid Mech.* 67: 19–47.
- 132 Maklad, O. and Poole, R.J. (2021). *J. Non-Newtonian Fluid Mech.* 292: 104522.
- 133 Weissenberg, K. (1947). *Nature* 159 (4035): 310–311.
- 134 Joseph, D.D. (1990). *Fluid Dynamics of Viscoelastic Liquids*, vol. 84. New York: Springer-Verlag.
- 135 Han, C.D. and Segal, L. (1970). *J. Appl. Polym. Sci.* 14 (12): 2973–2998.
- 136 McKay, G.R., Ferguson, J., and Hudson, N.E. (1978). *J. Non-Newtonian Fluid Mech.* 4 (1–2): 89–98.
- 137 Hsiao, K.W., Dinic, J., Ren, Y. et al. (2017). *Phys. Fluids* 29 (12): 121603.
- 138 Walter, A.V., Jimenez, L.N., Dinic, J. et al. (2019). *Rheol. Acta* 58: 145–157.
- 139 Dealy, J.M., Read, D.J., and Larson, R.G. (2018). *Structure and Rheology of Molten Polymers: from Structure to Flow Behavior and Back Again*. Carl Hanser Verlag GmbH Co KG.
- 140 Rouse, P.E. Jr. (1953). *J. Chem. Phys.* 21 (7): 1272–1280.
- 141 Zimm, B.H. (1956). *J. Chem. Phys.* 24: 269–278.
- 142 Bird, R.B., Armstrong, R.C., and Hassager, O. (1987). *Dynamics of Polymeric Liquids*, 2e, vol. 1. New York: John Wiley & Sons.
- 143 Prabhakar, R., Prakash, J.R., and Sridhar, T. (2006). *J. Rheol.* 50 (6): 925–947.
- 144 Fischer, P. and Windhab, E.J. (2011). *Curr. Opin. Colloid Interface Sci.* 16 (1): 36–40.
- 145 Tirtaatmadja, V. and Sridhar, T. (1993). *J. Rheol.* 37 (6): 1081–1102.
- 146 Huang, Q., Mednova, O., Rasmussen, H.K. et al. (2013). *Macromolecules* 46 (12): 5026–5035.
- 147 Huang, Q., Hengeller, L., Alvarez, N.J., and Hassager, O. (2015). *Macromolecules* 48 (12): 4158–4163.
- 148 Narimissa, E., Huang, Q., and Wagner, M.H. (2020). *J. Rheol.* 64 (1): 95–110.
- 149 Dontula, P., Pasquali, M., Scriven, L., and Macosko, C.W. (1997). *Rheol. Acta* 36 (4): 429–448.
- 150 Cooper-White, J.J., Crooks, R.C., Chockalingam, K., and Boger, D.V. (2002). *Ind. Eng. Chem. Res.* 41 (25): 6443–6459.
- 151 Plog, J.P., Kulicke, W.M., and Clasen, C. (2005). *Appl. Rheol.* 15 (1): 28–37.
- 152 Vadodaria, S.S. and English, R.J. (2016). *Cellulose* 23 (1): 339–355.

- 153 Chen, Y.-J. and Steen, P.H. (1997). *J. Fluid Mech.* 341: 245–267.
- 154 Day, R.F., Hinch, E.J., and Lister, J.R. (1998). *Phys. Rev. Lett.* 80 (4): 704–707.
- 155 Papageorgiou, D.T. (1995). *Phys. Fluids* 7: 1529–1544.
- 156 McKinley, G.H. and Tripathi, A. (2000). *J. Rheol.* 44 (3): 653–670.
- 157 Castrejón-Pita, J.R., Castrejón-Pita, A.A., Thete, S.S. et al. (2015). *Proc. Natl. Acad. Sci. U.S.A.* 112 (15): 4582–4587.
- 158 Renardy, M. (2004). *Rheol. Rev.* 2: 171–196.
- 159 Doshi, P. and Basaran, O.A. (2004). *Phys. Fluids* 16 (3): 585–593.
- 160 Suryo, R. and Basaran, O.A. (2006). *J. Non-Newtonian Fluid Mech.* 138 (2): 134–160.
- 161 Entov, V.M. and Yarin, A.L. (1984). *Fluid Dyn.* 19 (1): 21–29.
- 162 Renardy, M. (2002). *J. Non-Newtonian Fluid Mech.* 104 (1): 65–74.
- 163 Renardy, M. (2002). *J. Non-Newtonian Fluid Mech.* 103 (2–3): 261–269.
- 164 Renardy, M. (1995). *J. Non-Newtonian Fluid Mech.* 59 (2–3): 267–282.
- 165 Fontelos, M.A. and Li, J. (2004). *J. Non-Newtonian Fluid Mech.* 118 (1): 1–16.
- 166 Wagner, C., Bourouiba, L., and McKinley, G.H. (2015). *J. Non-Newtonian Fluid Mech.* 218: 53–61.
- 167 Oliveira, M.S.N. and McKinley, G.H. (2005). *Phys. Fluids* 17 (7): 071704; 1–4.
- 168 Oliveira, M.S.N., Yeh, R., and McKinley, G.H. (2006). *J. Non-Newtonian Fluid Mech.* 137 (1–3): 137–148.
- 169 Campo-Deano, L. and Clasen, C. (2010). *J. Non-Newtonian Fluid Mech.* 165 (23): 1688–1699.
- 170 Erni, P., Varagnat, M., Clasen, C. et al. (2011). *Soft Matter* 7 (22): 10889–10898.
- 171 Mathues, W., Formenti, S., McIlroy, C. et al. (2018). *J. Rheol.* 62 (5): 1135–1153. doi: 10.1122/1.5021834.
- 172 Khandavalli, S., Sharma-Nene, N., Kabir, S. et al. (2021). *ACS Appl. Polym. Mater.* 3 (5): 2374–2384.
- 173 Lang, C., Hendricks, J., Zhang, Z. et al. (2019). *Soft Matter* 15 (5): 833–841.
- 174 Rosello, M., Sur, S., Barbet, B., and Rothstein, J.P. (2019). *J. Non-Newtonian Fluid Mech.* 266: 160–170.
- 175 Zhou, J. and Doi, M. (2018). *Phys. Rev. Fluids* 3 (8): 084004.
- 176 Arnolds, O., Buggisch, H., Sachsenheimer, D., and Willenbacher, N. (2010). *Rheol. Acta* 49 (11–12): 1207–1217.
- 177 Clasen, C. (2010). *Korea-Australia Rheol. J.* 22 (4): 331–338.
- 178 Marshall, K.A., Liedtke, A.M., Todt, A.H., and Walker, T.W. (2017). *Exp. Fluids* 58: 69. doi: 10.1007/s00348-017-2351-9.
- 179 Suteria, N.S., Gupta, S., Potineni, R. et al. (2019). *Rheol. Acta* 58: 403–417.
- 180 Marshall, K.A. and Walker, T.W. (2019). *Rheol. Acta* 58 (9): 573–590.
- 181 Murdoch, T.J., Pashkovski, E., Patterson, R. et al. (2020). *ACS Appl. Polym. Mater.* 2 (9): 4062–4070.
- 182 Su, Y., Palacios, B., and Zenit, R. (2021). *Phys. Rev. Fluids* 6 (3): 033303.
- 183 Franco-Gómez, A., Onuki, H., Yokoyama, Y. et al. (2021). *Exp. Fluids* 62 (2): 1–15.
- 184 Gupta, S. and Vanapalli, S.A. (2020). *Phys. Fluids* 32 (1): 012006.

- 185 Zhang, Y. and Muller, S.J. (2018). *Phys. Rev. Fluids* 3 (4): 043301. doi: 10.1103/PhysRevFluids.3.043301.
- 186 Wu, S.J. and Mohammadigoushki, H. (2018). *J. Rheol.* 62 (5): 1061–1069. doi: 10.1122/1.5031899.
- 187 Omidvar, R., Wu, S., and Mohammadigoushki, H. (2019). *J. Rheol.* 63 (1): 33–44.
- 188 Wu, S. and Mohammadigoushki, H. (2020). *Phys. Rev. Fluids* 5 (5): 053303.
- 189 Dinic, J. and Sharma, V. (2020). *Macromolecules* 53: 3424–3437.
- 190 Pincus, P. (1976). *Macromolecules* 9 (3): 386–388.
- 191 Pincus, P. (1977). *Macromolecules* 10 (1): 210–213.
- 192 Unidad, H.J., Goad, M.A., Bras, A.R. et al. (2015). *Macromolecules* 48 (18): 6638–6645. doi: 10.1021/acs.macromol.5b00341.
- 193 Fetters, L.J., Lohse, D.J., Milner, S.T., and Graessley, W.W. (1999). *Macromolecules* 32 (20): 6847–6851.
- 194 Shenoy, S.L., Bates, W.D., Frisch, H.L., and Wnek, G.E. (2005). *Polymer* 46 (10): 3372–3384.
- 195 Gupta, P., Elkins, C., Long, T.E., and Wilkes, G.L. (2005). *Polymer* 46 (13): 4799–4810.
- 196 McKee, M.G., Wilkes, G.L., Colby, R.H., and Long, T.E. (2004). *Macromolecules* 37 (5): 1760–1767.
- 197 Gupta, V.B. and Kothari, V.K. (1997). *Manufactured Fiber Technology*. London: Chapman & Hall.
- 198 Zhang, X. and Lu, Y. (2014). *Polym. Rev.* 54 (4): 677–701.
- 199 Fang, Y., Dulaney, A.R., Gadley, J. et al. (2016). *Polymer* 88: 102–111.
- 200 Merchiers, J., Martínez Narváez, C.D.V., Slykas, C. et al. (2021). *J. Polym. Sci.* doi: 10.1002/pol.20210424.
- 201 Atıcı, B., Ünlü, C.H., and Yanilmaz, M. (2021). *Polym. Rev.* 12: 1–64.
- 202 Park, J.H. and Rutledge, G.C. (2017). *Macromolecules* 50 (15): 5627–5642.
- 203 Latinwo, F. and Schroeder, C.M. (2011). *Soft Matter* 7 (18): 7907–7913.
- 204 Tree, D.R., Muralidhar, A., Doyle, P.S., and Dorfman, K.D. (2013). *Macromolecules* 46 (20): 8369–8382.
- 205 Flory, P.J. (1956). *Proc. R. Soc. Lond. A* 234 (1196): 60–73.
- 206 Broedersz, C.P. and MacKintosh, F.C. (2014). *Rev. Mod. Phys.* 86 (3): 995.
- 207 Odijk, T. (1983). *Macromolecules* 16 (8): 1340–1344.
- 208 Morse, D. and Viscoelasticity, C. (1998). *Macromolecules* 31 (20): 7030–7043.
- 209 Frey, E., Kroy, K., and Wilhelm, J. (1999). Sudarshan K. Malhotra, Jack A. Tuszyński, In: *Advances in Structural Biology* (eds. Sudarshan K. Malhotra, Jack A. Tuszyński). vol. 5, 135–168. Elsevier.
- 210 Krishna Reddy, N., Zhang, Z., Paul Lettinga, M. et al. (2012). *J. Rheol.* 56 (5): 1153–1174.
- 211 Tanner, R.I. (1975). *Trans. Soc. Rheol.* 19 (4): 557–582.
- 212 Hinch, E.J. (1977). *Phys. Fluids* 20 (10): S22–S30.
- 213 Fuller, G.G. and Leal, L.G. (1980). *Rheol. Acta* 19 (5): 580–600.
- 214 Wiest, J.M., Wedgewood, L.E., and Bird, R.B. (1989). *J. Chem. Phys.* 90 (1): 587–594.

- 215 Schroeder, C.M., Shaqfeh, E.S.G., and Chu, S. (2004). *Macromolecules* 37 (24): 9242–9256. doi: 10.1021/ma049461l.
- 216 Hsieh, C.C. and Larson, R.G. (2004). *J. Rheol.* 48 (5): 995–1021. doi: 10.1122/1.1781171.
- 217 Hsieh, C.C. and Larson, R.G. (2005). *J. Rheol.* 49 (5): 1081–1089. doi: 10.1122/1.2000971.
- 218 Hsieh, C.C., Li, L., and Larson, R.G. (2003). *J. Non-Newtonian Fluid Mech.* 113 (2–3): 147–191. doi: 10.1016/s0377-0257(03)00107-1.
- 219 Fetters, L.J., Lohse, D.J., and Colby, R.H. (2007). James E. Mark In: *Physical Properties of Polymers Handbook* (ed. James E. Mark), 447–454. Springer.
- 220 Witten, T.A., Milner, S.T., and Wang, Z.G. (1989). In: *Multiphase Macromolecular Systems* (ed. B.M. Culbertson). New York: Plenum.
- 221 Qin, J. and Milner, S.T. (2013). *Macromolecules* 46 (4): 1659–1672.
- 222 Horinaka, J., Chen, K., and Takigawa, T. (2018). *Rheol. Acta* 57 (1): 51–56. doi: 10.1007/s00397-017-1053-9.
- 223 Horinaka, J., Yasuda, R., and Takigawa, T. (2011). *J. Polym. Sci. Part B Polym. Phys.* 49 (13): 961–965. doi: 10.1002/polb.22262.
- 224 Del Giudice, F., Tassieri, M., Oelschlaeger, C., and Shen, A.Q. (2017). *Macromolecules* 50 (7): 2951–2963.
- 225 Mathues, W., Shahid, T., Hendricks, J., and Clasen, C. (2016). *Rheol. Bull.* 57 (3): 57–62.
- 226 Odijk, T. (2017). *Polymers* 9 (6): 190.
- 227 Radhakrishnan, R. and Underhill, P.T. (2012). *Macromolecules* 46 (2): 548–554.
- 228 Sridhar, T., Nguyen, D.A., Prabhakar, R., and Prakash, J.R. (2007). *Phys. Rev. Lett.* 98 (16): 167801. doi: 10.1103/PhysRevLett.98.167801.
- 229 Stoltz, C., de Pablo, J.J., and Graham, M.D. (2006). *J. Rheol.* 50 (2): 137–167.
- 230 Fuller, G.G., Cathey, C.A., Hubbard, B., and Zebrowski, B.E. (1987). *J. Rheol.* 31 (3): 235–249.
- 231 Arfin, N. and Bohidar, H.B. (2012). *Int. J. Biol. Macromol.* 50 (3): 759–767.
- 232 Martínez-Richa, A. (2012). *Carbohydr. Polym.* 87 (3): 2129–2136.